A new certification framework for the port reduced static condensation reduced basis element method

Kathrin Smetana

Department of Mechanical Engineering, Massachusetts Institute of Technology, 77 Massachusetts Avenue, Cambridge, MA-02139, USA

Abstract

In this paper we introduce a new certification framework for the port-reduced static condensation reduced basis element (PR-SCRBE) method, which has been developed for the simulation of large component based applications such as bridges or acoustic waveguides. In an offline computational stage we construct a library of interoperable parametrized reference components; in the subsequent online stage we instantiate and connect the components at the interfaces/ports to form a system of components. To compute a "truth" finite element approximation of the (say) coercive elliptic partial differential equation on the component based system we use a domain decomposition approach. For an efficient simulation we employ two different types of model reduction — a reduced basis (RB) approximation within the interior of the component (Huynh et al. 2013) and empirical port reduction (Eftang and Patera 2013) on the ports where the components connect.
We demonstrate the well-posedness of the PR-SCRBE approximation and introduce a new certification framework. To assess the quality of the port reduction we use conservative fluxes. We adapt the standard estimators from RB methods to the SCRBE setting to derive an a posteriori error estimator for the RB-error contribution. In order to combine the a posteriori estimators for both error contributions and derive a rigorous a posteriori error estimator for PR-SCRBE we adapt techniques from multi-scale methods and component mode synthesis. Finally, we prove that the effectivity of the derived estimator can be bounded.
We provide numerical experiments for heat conduction and linear elasticity to show that the derived a posteriori error estimator provides an effective estimator. Moreover we demonstrate the applicability of the introduced certification framework by analyzing the computational (online) costs.

Keywords: A posteriori error estimation, domain decomposition, reduced basis methods
2000 MSC: 65N15, 65N30, 65N55, 65N12

1. Introduction

Within many engineering applications the considered structure allows for a natural decomposition in components. Examples are bridges, buildings, aircrafts, oil and gas platforms, musical instruments or mufflers. One popular method for the simulation and analysis of such large engineering systems is component mode synthesis (CMS). The CMS approach introduced in [1, 2] uses the eigenmodes of local constrained eigenvalue problems for the approximation within the interior of the component and static condensation to arrive at a (Schur complement) system associated with the coupling modes on the interfaces or ports. In more recent works also the static or coupling modes are chosen as eigenmodes [3, 4, 5] and used within an adaptive scheme

Email address: ksmetana@mit.edu (Kathrin Smetana)

Report Documentation Page

Form Approved
OMB No. 0704-0188

1. REPORT DATE	2. REPORT TYPE	3. DATES COVERED
04 SEP 2014		**00-00-2014 to 00-00-2014**

4. TITLE AND SUBTITLE	5a. CONTRACT NUMBER
A new certification framework for the port reduced static condensation reduced basis element method	5b. GRANT NUMBER
	5c. PROGRAM ELEMENT NUMBER
6. AUTHOR(S)	5d. PROJECT NUMBER
	5e. TASK NUMBER
	5f. WORK UNIT NUMBER
7. PERFORMING ORGANIZATION NAME(S) AND ADDRESS(ES)	8. PERFORMING ORGANIZATION REPORT NUMBER
Massachusetts Institute of Technology,Department of Mechanical Engineering,77 Massachusetts Avenue,Cambridge,MA,02139	
9. SPONSORING/MONITORING AGENCY NAME(S) AND ADDRESS(ES)	10. SPONSOR/MONITOR'S ACRONYM(S)
	11. SPONSOR/MONITOR'S REPORT NUMBER(S)

12. DISTRIBUTION/AVAILABILITY STATEMENT

Approved for public release; distribution unlimited

13. SUPPLEMENTARY NOTES

14. ABSTRACT

In this paper we introduce a new certification framework for the port-reduced static condensation reduced basis element (PR-SCRBE) method, which has been developed for the simulation of large component based applications such as bridges or acoustic waveguides. In an offline computational stage we construct a library of interoperable parametrized reference components; in the subsequent online stage we instantiate and connect the components at the interfaces/ports to form a system of components. To compute a ?truth? finite element approximation of the (say) coercive elliptic partial differential equation on the component based system we use a domain decomposition approach. For an efficient simulation we employ two different types of model reduction ? a reduced basis (RB) approximation within the interior of the component (Huynh et al. 2013) and empirical port reduction (Eftang and Patera 2013) on the ports where the components connect. We demonstrate the well-posedness of the PR-SCRBE approximation and introduce a new certification framework. To assess the quality of the port reduction we use conservative fluxes. We adapt the standard estimators from RB methods to the SCRBE setting to derive an a posteriori error estimator for the RBerror contribution. In order to combine the a posteriori estimators for both error contributions and derive a rigorous a posteriori error estimator for PR-SCRBE we adapt techniques from multi-scale methods and component mode synthesis. Finally, we prove that the effectivity of the derived estimator can be bounded. We provide numerical experiments for heat conduction and linear elasticity to show that the derived a posteriori error estimator provides an effective estimator. Moreover we demonstrate the applicability of the introduced certification framework by analyzing the computational (online) costs.

15. SUBJECT TERMS

16. SECURITY CLASSIFICATION OF:			17. LIMITATION OF ABSTRACT	18. NUMBER OF PAGES	19a. NAME OF RESPONSIBLE PERSON
a. REPORT **unclassified**	b. ABSTRACT **unclassified**	c. THIS PAGE **unclassified**	**Same as Report (SAR)**	**36**	

Standard Form 298 (Rev. 8-98)
Prescribed by ANSI Std Z39-18

based on a posteriori error estimators [5]. One drawback of the CMS approach is the rather slow convergence of eigenmodal expansions. In contrast the reduced basis element (RBE) method [6] employs a reduced basis expansion [7] within each component or subdomain and Lagrange multipliers to couple the local bases and hence compute a global solution of the considered parameter dependent partial differential equation for each admissible parameter. The RBE method thus profits from the fact that RB approximations yield a rapid and in many cases exponential convergence [8].
A combination of RB methods and domain decomposition approaches has for instance also been considered in [9, 10]. Similarly RB methods have been employed in the framework of a multi-scale finite element method to construct local reduced spaces for the approximation of fine-scale features on the coarse grid elements in [11, 12, 13], where the latter corresponds to the "components" in the RBE method.
In this paper we consider the port reduced static condensation reduced basis element (PR-SCRBE) method [14, 15] which combines ideas of the CMS and the RBE method. SCRBE as introduced in [14] has been successfully applied amongst others to heat exchanger systems [16] and musical instruments and mufflers [17] and PR-SCRBE introduced in [15] to heat transfer [15] and large structures in linear elasticity [18]. A key advantage of the PR-SCRBE method is its "bottom-up" approach from an offline-prepared library of completely interchangeable and interoperable parametrized components to many different online-formed global systems of components. To construct rapid convergent reduced bases we use an RB approximation in the component interior [14] and empirical port reduction based on RB techniques [15] on the ports, while the coupling is realized by applying static condensation. More precisely, we first compute coupling modes as the harmonic liftings of the empirical port modes. Subsequently, we compute RB approximations of the component interior "bubble" functions, each associated with a different coupling mode, which solve the parameter dependent PDE within each component and hence account for material or geometric parameters. Employing a different RB approximation for each bubble function yields a rapid convergent and computationally efficient approximation.
The main contribution of this paper is the introduction of a new certification framework for the PR-SCRBE method which provides a rigorous and effective a posteriori error estimator of the error between the PR-SCRBE approximation and the "truth" finite element approximation on the global system in an energy norm. We adapt techniques from RB methods [7] to derive an a posteriori error estimator for the RB error of the bubble approximation in the component interior by considering weighted Riesz representations. To derive an a posteriori error estimator for port reduction we adapt the concept of conservative fluxes introduced in Hughes et al. [19] to the PR-SCRBE setting. We compute weak fluxes of the PR-SCRBE approximation on each port with respect to the full port space and employ the jumps to define an a posteriori error estimator for port reduction. Thanks to the weak flux continuity of the "truth" solution the proposed estimator thus measures how well the PR-SCRBE approximation behaves like the "truth" solution on the ports. We remark that the concept of conservative fluxes has been used as an error indicator in the formulation of an adaptive variational multi-scale method in [20] and an adaptive multi-scale finite element method in [21] to determine the computational domains for the local fine scale problems. To combine both error estimators we exploit that due to the fact that the coupling modes are chosen as harmonic extensions the span of the coupling modes and the span of the bubble functions for each component are orthogonal. Orthogonality with respect to the bilinear form has been exploited for the derivation of an a posteriori error estimator for the CMS approach in [5]. In the recently introduced local orthogonal decomposition method [22] the coarse and fine scale spaces are constructed in such a way that orthogonality with respect to the bilinear form is obtained and then exploited for an error analysis.
Our a posteriori error estimator features several important innovations. First, in contrast to earlier contributions [14, 15, 18], it provides an estimator for the energy norm of the error. Second, its validity does not rely on the quality of the RB approximation, whereas the estimator proposed in [14] provides only a rigorous bound if the sum over the RB-error in the entries of the Schur complement matrix is smaller than

the smallest eigenvalue of the "truth" Schur complement matrix. Moreover, the error estimator is based on local component-wise element indicators and may hence be employed within an adaptive PR-SCRBE scheme. Note that in contrast the a posteriori error estimator proposed for the CMS approach in [5] relies on a weak residual with respect to the global port space. For the localized reduced basis multi-scale method an a posteriori bound using local error indicators based on conforming flux reconstruction is stated in [23]. We also derive upper bounds for the effectivities both of the error estimator and the local indicators. Finally, we demonstrate in numerical experiments that the derived estimator is also computationally efficient as its computation requires only relatively small additional online costs in comparison to the computation of the PR-SCRBE approximation.
The remaining part of this paper is organized as follows. In Section 2 we describe the parametrized component based static condensation framework as introduced in [14]. In the following Section 3 we present the PR-SCRBE method [14, 15] and prove well-posedness of the PR-SCRBE approximation. The main new contribution of this paper is developed in Section 4 where we derive the a posteriori error estimator and prove its effectivity. Subsequently we discuss the computational costs both of the PR-SCRBE approximation and the introduced error estimator in Section 5. Finally, we present numerical experiments for heat conduction and linear elasticity in Section 6 to validate the theoretical results and draw some conclusions in Section 7.

2. Component based static condensation

The key concepts of the PR-SCRBE approximation are a *library* of parametrized archetype components associated with reference domains and a parametrized PDE (§2.1.1) and a *system* of instantiated components, mapped to their physical coordinates and connected at ports (§2.1.2). Each archetype component represents a specific geometric form, for instance a beam or a fin, and may feature various ports of different types. To simplify the notation we will however consider in this paper only one archetype component and one port type.
To compute a numerical approximation of the parametrized PDE for the global system we employ a (multi-domain) domain decomposition approach and eliminate degrees of freedom in the component interior by static condensation (§2.2).

2.1. Component library

2.1.1. Archetype (reference) component

The considered archetype component is associated with a bounded reference domain $\widehat{\Omega} \subset \mathbb{R}^d$, $d = 1, 2, 3$ with Lipschitz boundary $\partial\widehat{\Omega}$. It is equipped with P^γ local ports $\hat{\gamma}_j \subset \partial\widehat{\Omega}$, $j = 1, ..., P^\gamma$ at which instantiations of this archetype components can be connected in the online stage as depicted in Fig. 1. We assume that local ports are mutually separated by manifolds $\Sigma \subset \partial\widehat{\Omega}$ with positive Hausdorff measure. For the treatment of systems of components with intersecting ports we refer to [4].
Furthermore, we associate with the archetype component a parametrized PDE modeling the physical phenomena of the target application. To formulate the corresponding variational problem we introduce an archetype continuous bilinear form $\hat{a}(\cdot, \cdot; \hat{\mu}) : \hat{X} \times \hat{X} \to \mathbb{R}$ and a continuous linear functional $\hat{f}(\cdot; \hat{\mu}) : \hat{X} \to \mathbb{R}$, where $(H_0^1(\widehat{\Omega}))^{d_r} \subset \hat{X} \subset (H^1(\widehat{\Omega}))^{d_r}$. Here, $\hat{\mu} \in \widehat{\mathcal{D}} \subset \mathbb{R}^z$ denotes a parameter vector which describes for instance a material parameter as Young's modulus or modifies the geometry of the component say via a dilation and $\widehat{\mathcal{D}}$ is the corresponding z-dimensional parameter space. Moreover, d_r equals one for scalar valued and d for vector valued parametrized PDEs and Dirichlet boundary conditions may be only prescribed on ports. We assume an affine parameter dependence of $\hat{a}(\cdot, \cdot; \hat{\mu})$ and $\hat{f}(\cdot; \hat{\mu})$, i.e.

$$\hat{a}(\cdot, \cdot; \hat{\mu}) = \sum_{q=1}^{\hat{Q}^a} \hat{\theta}_q^a(\hat{\mu}) \hat{a}^q(\cdot, \cdot) \quad \text{and} \quad \hat{f}(\cdot; \hat{\mu}) = \sum_{q=1}^{\hat{Q}^f} \hat{\theta}_q^f(\hat{\mu}) \hat{f}^q(\cdot), \tag{1}$$

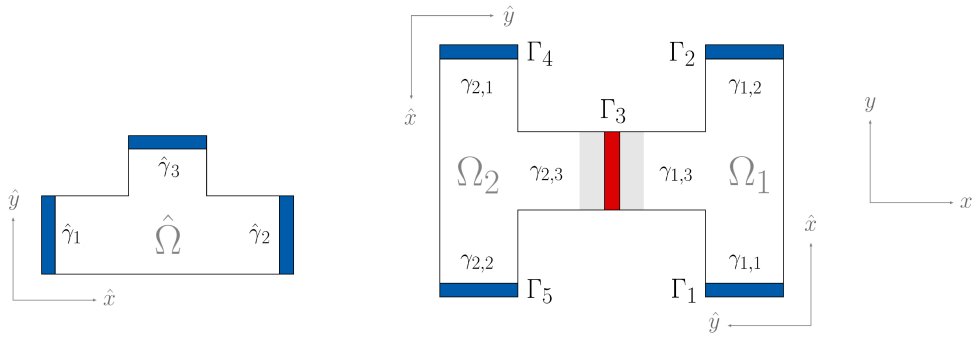

(a) archetype (reference) component (b) system of two rotated and deformed components

Figure 1: A library with one archetype component (a): The archetype reference domain is $\widehat{\Omega}$ and the archetype component has $P^\gamma = 3$ local ports $\hat{\gamma}_j$, $j = 1, .., 3$. A system of $I = 2$ components 1 and 2 which are instantiations of the archetype (b): The component domains are $\Omega = \mathcal{T}_1(\widehat{\Omega})$ and $\Omega_2 = \mathcal{T}_2(\widehat{\Omega})$ and the components are connected at the global port Γ_3. Thus we have for instance $\pi_1 = \{(1,1)\}, \pi_2 = \{(1,2)\}, \pi_3 = \{(1,3),(2,3)\}$ and conversely $\Pi_1(1) = 1, \Pi_1(2) = 2$ and $\Pi_1(3) = \Pi_2(3) = 3$. Both mappings $\mathcal{T}_i$, $i = 1, 2$ are compositions of a rotation $\mathcal{T}_i^{rot}$ and a dilation $\mathcal{T}_i^{def}$, $i = 1, 2$ indicated by the shading in gray. Note that thanks to the application of $\mathcal{T}_i^{map}$ to the dependent variables we obtain a field in the physical system coordinates which has the same spatial orientation as in the coordinate system of the archetype reference component.

where $\hat{a}^q(\cdot,\cdot) : \hat{X} \times \hat{X} \to \mathbb{R}$, $q = 1, ..., \hat{Q}^a$ and $\hat{f}^q(\cdot) : \hat{X} \to \mathbb{R}$, $q = 1, ..., \hat{Q}^f$ are parameter independent bilinear and linear forms, and $\hat{\theta}_q^a$ and $\hat{\theta}_q^f$ are parameter dependent functions. For general parameter dependent forms an (empirical) interpolation [24] may be invoked to realize an (approximate) affine decomposition. Furthermore, we define an inner product and the corresponding, induced norm as

$$(\cdot,\cdot)_{\hat{X}} : \hat{X} \times \hat{X} \to \mathbb{R} \quad \text{and} \quad \|\cdot\|_{\hat{X}} := \sqrt{(\cdot,\cdot)_{\hat{X}}}.$$

We require $\|\cdot\|_{\hat{X}}$ to be a semi-norm on $(H^1(\widehat{\Omega}))^{d_r}$ and a full norm on the space $\{\hat{v} \in (H^1(\widehat{\Omega}))^{d_r} : v|_{\hat{\gamma}_j} = 0$ for at least one $j \in \{1, ..., P^\gamma\}\}$. For notational convenience we also introduce a (geometric) parameter-dependent inner product on the archetype component as $(\cdot,\cdot;\hat{\mu})_{\hat{X};\hat{\mu}} : \hat{X} \times \hat{X} \to \mathbb{R}$ and the induced norm $\|v\|_{\hat{X};\hat{\mu}} := ((v,v;\hat{\mu})_{\hat{X};\hat{\mu}})^{1/2}$ for $v \in \hat{X}$. Finally, we introduce "truth" archetype finite element (FE) spaces $\hat{X}^{\mathcal{N}} \subset \hat{X}$ of dimension $\mathcal{N}$. For each local port within an archetype component we introduce the trace space $\hat{\Lambda}_j = \{\nu \in H^{1/2}(\hat{\gamma}_j) : \nu = v|_{\hat{\gamma}_j}, v \in \hat{X}\}$ and its discrete counterpart — the discrete port space

$$\hat{\Lambda}_j^{\mathcal{N}_\mathcal{P}} := X^{\mathcal{N}}|_{\hat{\gamma}_j} = \text{span}\{\hat{\chi}_{j,1}, ..., \hat{\chi}_{j,\mathcal{N}_\mathcal{P}}\}, \quad j = 1, ..., P^\gamma, \tag{2}$$

of dimension $\mathcal{N}_\mathcal{P}$ with basis $\{\hat{\chi}_{j,k}\}_{k=1}^{\mathcal{N}_\mathcal{P}}$.

2.1.2. System

In the online stage we form the target structure, say a bridge or an electronic module, and hence a global system of I components mapped to physical (system) coordinates. Each component i, $i = 1, ..., I$ is instantiated from one archetype component as assumed in the beginning of this section. We also introduce the parameter vector $\mu_i \in \mathcal{D}_i \subset \hat{\mathcal{D}}$. Note that $\mathcal{D}_i$ differs between distinct components in the global system if we prescribe for instance a traction on one end of a beam structure as in Subsection 6.2. We may then define

an affine parameter dependent geometric transformation $\mathcal{T}_i : \widehat{\Omega} \to \Omega_i$ from (archetype) reference to physical (system) coordinates, where we denote with $\Omega_i = \mathcal{T}_i(\widehat{\Omega})$ the instantiated and transformed component domain. Accordingly $\gamma_{i,j} = \mathcal{T}_i(\hat{\gamma}_j)$, $j = 1, ..., P^\gamma$ are the transformed ports. We assume that $\mathcal{T}_i$ is a composition of a deformation $\mathcal{T}_i^{def}$ and a rotation $\mathcal{T}_i^{rot}$, i.e. $\mathcal{T}_i = \mathcal{T}_i^{rot}\mathcal{T}_i^{def}$ with $\mathcal{T}_i^{def}(\hat{x}) = G_i\hat{x} + t_i$, $\hat{x} \in \widehat{\Omega}$. Here, $G_i \in \mathbb{R}^{d\times d}$ is the Jacobian of $\mathcal{T}_i^{def}$ and $t_i \in \mathbb{R}^d$ is a translation vector. Hence, $\mathcal{T}_i^{def}$ may describe a composition of (say) a dilation and a translation, but rotations are not permitted. In this paper we assume that Ω_i and hence $\mathcal{T}_i$ do not degenerate. Moreover, we suppose that $\mathcal{T}_i$ when applied to a port is a pure rigid body transformation, i.e. a composition of a rotation and translation, which is for instance fulfilled for the mappings in Fig. 1. Details on the difficulties that arise when this assumption is dropped and possible solutions are provided below.

Next we define the global (system) domain Ω as $\bar{\Omega} = \cup_{i=1}^I \bar{\Omega}_i$ and recall that the instantiated and transformed components are connected at their ports. More precisely we say that two components i and i' are connected at a global port Γ_p if $\bar{\Omega}_i \cap \bar{\Omega}_{i'} = \Gamma_p$. We register those connections in a global-to-local index set $\pi_p = \{(i,j),(i',j')\}$ which contains also the indices of the respective local ports $\gamma_{i,j}$ and $\gamma_{i',j'}$ at which the components i and i' connect. Note that a global port may also lie on $\partial\Omega$ and is then only associated with one local port $\gamma_{i,j}$ of component i; hence we set $\pi_p = \{(i,j)\}$ in this case. Additionally we introduce for each instantiated component i, $i = 1, ..., I$, a local-to-global port map Π_i, which is defined as $\Pi_i(j) = p$ if $(i,j) \in \pi_p$, $j = 1, ..., P^\gamma$ and $p = 1, ..., P_0^\Gamma$ as illustrated in Fig. 1. Here, P_0^Γ is the number of global ports in the system. Finally, we denote with $P^\Gamma \leq P_0^\Gamma$ the number of global ports on which we do not impose Dirichlet conditions.

To define a "truth" FE solution for the global system we first introduce for each component i, $i = 1, ..., I$ a mapped FE space

$$X_i^{\mathcal{N}} := \text{span}\{\mathcal{T}_i^{map}(v \circ \mathcal{T}_i^{-1}), \;\; v \in \hat{X}^{\mathcal{N}}\}, \tag{3}$$

where $\mathcal{T}_i^{map} = \mathcal{T}_i^{rot}$ for vector-valued functions and $\mathcal{T}_i^{map}$ equals the identity map for scalar-valued functions. We emphasize that we should instead use the notation $X_i^{\mathcal{N}}(\mu_i)$, but to improve readability we omit here and henceforth the argument μ for spaces that depend (merely) on the geometrical parameters. Next, we introduce for $i = 1, ..., I$ and $j = 1, ..., P^\gamma$ a mapped discrete port space

$$\Lambda_{i,j}^{\mathcal{N}_\mathcal{P}} := \text{span}\{\chi_{i,j,k}, \;\; k = 1, ..., \mathcal{N}_\mathcal{P}\} \quad \text{with} \quad \chi_{i,j,k} := \mathcal{T}_i^{map}(\hat{\chi}_{j,k} \circ \mathcal{T}_i^{-1}). \tag{4}$$

To obtain continuity of the global solution it is essential to require compatible port spaces in the sense that

$$\chi_{i,j,k} = \chi_{i',j',k} \quad \text{for} \quad \pi_p = \{(i,j),(i',j')\} \tag{5}$$

for all global ports Γ_p within the global system at which two components connect. One key point to satisfy (5) is to define the (archetype) port spaces $\hat{\Lambda}_j^{\mathcal{N}_\mathcal{P}}$ according to the orientation of the respective (archetype) port $\hat{\gamma}_j$ within the component. Moreover, for vector-valued functions the application of $\mathcal{T}_i^{rot}$ to the dependent variables (see (3) and (4)) ensures the right orientation of the mapped port space $\Lambda_{i,j}^{\mathcal{N}_\mathcal{P}}$ in the global system. We refer to [18] for a detailed discussion of the port compatibility requirement (5) in the case of vector-valued functions.

We may now introduce a global solution space $(H_0^1(\Omega))^{d_r} \subset X \subset (H^1(\Omega))^{d_r}$ and a global FE space $X^{\mathcal{N}} \subset X$ as $X^{\mathcal{N}} = \oplus_{i=1}^I X_i^{\mathcal{N}}$. We only consider homogeneous Dirichlet boundary conditions as non-homogeneous Dirichlet boundary conditions may be treated as usual by employing a lifting function. Furthermore, we define for any system parameter vector $\mu = (\mu_1, ..., \mu_I) \in \mathcal{D} = \prod_{i=1}^I \mathcal{D}_i$ a bilinear form $a(\cdot,\cdot;\mu) : X \times X \to \mathbb{R}$

and a linear functional $f(\cdot;\mu) : X \to \mathbb{R}$ as

$$a(w,v;\mu) := \sum_{i=1}^{I} a_i(w,v;\mu_i), \quad \text{with}$$

$$a_i(w,v;\mu_i) := \hat{a}((\mathcal{T}_i^{map})^{-1}(w|_{\Omega_i} \circ \mathcal{T}_i), (\mathcal{T}_i^{map})^{-1}(v|_{\Omega_i} \circ \mathcal{T}_i); \mu_i) \quad \forall w, v \in X, \tag{6}$$

$$f(v;\mu) := \sum_{i=1}^{I} f_i(v;\mu_i) \quad \text{with } f_i(v;\mu_i) := \hat{f}((\mathcal{T}_i^{map})^{-1}(v|_{\Omega_i} \circ \mathcal{T}_i); \mu_i) \quad \forall v \in X. \tag{7}$$

Note that the parameter dependent part of the entries and the determinant of the Jacobian $D\mathcal{T}_i$ of the mapping $\mathcal{T}_i$ are contained in μ_i, if necessary. If the material parameters do not depend on the spatial orientation of the component, the application of $\mathcal{T}_i^{rot}$ to the parameter dependent vector-valued functions results in a cancellation of $(\mathcal{T}_i^{rot})^{-1}$ in (6) thanks to $D\mathcal{T}_i = \mathcal{T}_i^{rot} G_i$. This therefore removes parameters which account for the spatial orientation of the component from the bilinear form. Note that for scalar-valued functions we obtain this cancellation thanks to the fact that $\mathcal{T}_i^{rot}$ is an orthogonal mapping. We also define an inner product and the induced norm as

$$(v,w)_X := \sum_{i=1}^{I} ((\mathcal{T}_i^{map})^{-1}(v|_{\Omega_i} \circ \mathcal{T}_i), (\mathcal{T}_i^{map})^{-1}(w|_{\Omega_i} \circ \mathcal{T}_i); \mu_i)_{\hat{X};\hat{\mu}}, \qquad \|v\|_X := \sqrt{(v,v)_X}. \tag{8}$$

Although both the inner product $(\cdot,\cdot)_X$ and the induced norm $\|\cdot\|_X$ depend on geometric parameters, we omit the dependency on the parameter μ in the definition to increase readability. We require that the bilinear form $a(\cdot,\cdot;\mu)$ is coercive and continuous on X with respect to the norm $\|\cdot\|_X$ and define the respective coercivity and continuity constants as follows

$$\alpha(\mu) := \inf_{v \in X} \frac{a(v,v;\mu)}{\|v\|_X^2} \quad \text{and} \quad \nu(\mu) := \sup_{v \in X} \sup_{w \in X} \frac{a(v,w;\mu)}{\|v\|_X \|w\|_X}. \tag{9}$$

Moreover we demand that $f(\cdot;\mu)$ is bounded with respect to $\|\cdot\|_X$ on X. Note that this implies coercivity and continuity of $\hat{a}(\cdot,\cdot;\hat{\mu})$ and boundedness of $\hat{f}(\cdot;\hat{\mu})$ with respect to the norm $\|\cdot\|_{\hat{X}}$. Finally, we define the coercivity and the continuity constants of $a(\cdot,\cdot,\mu)$ associated with the space $X^{\mathcal{N}}$ as

$$\alpha^{\mathcal{N}}(\mu) := \inf_{v \in X^{\mathcal{N}}} \frac{a(v,v;\mu)}{\|v\|_X^2} \quad \text{and} \quad \nu^{\mathcal{N}}(\mu) := \sup_{v \in X^{\mathcal{N}}} \sup_{w \in X^{\mathcal{N}}} \frac{a(v,w;\mu)}{\|v\|_X \|w\|_X}. \tag{10}$$

We may now formulate the global variational problem which reads as follows

$$\text{For any } \mu \in \mathcal{D}, \text{ find } u^e(\mu) \in X : \ a(u^e(\mu), v; \mu) = f(v;\mu), \quad \forall v \in X. \tag{11}$$

Moreover, we consider the following global "truth" finite element approximation

$$\text{For any } \mu \in \mathcal{D}, \text{ find } u(\mu) \in X^{\mathcal{N}} : \ a(u(\mu), v; \mu) = f(v;\mu), \quad \forall v \in X^{\mathcal{N}}. \tag{12}$$

Note that the port compatibility requirement (5) and our assumptions on $a(\cdot,\cdot;\mu)$ and $f(\cdot;\mu)$ ensure well-posedness of (11) and (12). We omit here and henceforth a super index $\mathcal{N}$ for functions in the possibly high-dimensional FE space $X^{\mathcal{N}}$ to improve readability.

2.2. Static condensation

To formulate the static condensation procedure we decompose $X^{\mathcal{N}}$ into a space corresponding to the component-interior, which we will call henceforth bubble space, and a skeleton space associated with ports. First, we define a bubble space on the archetype component as

$$\hat{B}^{\mathcal{N}} := \{v \in \hat{X}^{\mathcal{N}} \,:\, v|_{\hat{\gamma}_j} = 0,\ \ 1 \le j \le P^\gamma\},$$

and for each instantiated component a mapped bubble space

$$B_i^{\mathcal{N}} := \text{span}\{\mathcal{T}_i^{map}(w \circ \mathcal{T}_i^{-1}), \quad w \in \hat{B}^{\mathcal{N}}\}. \tag{13}$$

Finally, we introduce a global bubble space $B^{\mathcal{N}} := \bigoplus_{i=1}^{I} B_i^{\mathcal{N}}$. To define the skeleton space, we choose the coupling modes or interface functions $\hat{\psi}_{j,k} \in \hat{X}^{\mathcal{N}}$ as harmonic extensions of the port modes, i.e.

$$(\hat{\psi}_{j,k}, w)_{\hat{X}} = 0 \quad \forall w \in \hat{B}^{\mathcal{N}}, \qquad \hat{\psi}_{j,k} = \begin{cases} \hat{\chi}_{j,k}, & \text{on } \hat{\gamma}_j, \\ 0, & \text{on } \hat{\gamma}_{j'} \text{ for } j' \neq j, \end{cases}, \tag{14}$$

for $1 \le k \le \mathcal{N}_{\mathcal{P}}$, $1 \le j \le P^\gamma$. On instantiated components i, $1 \le i \le I$ we may then define $\psi_{i,j,k} \equiv \mathcal{T}_i^{map}(\hat{\psi}_{j,k} \circ \mathcal{T}_i^{-1})$. The global functions

$$\Psi_{p,k} := \begin{cases} \psi_{i',j',k}, & \text{in } \Omega_{i'}, \\ \psi_{i,j,k}, & \text{in } \Omega_i, \\ 0, & \text{in } \Omega \setminus (\Omega_{i'} \cup \Omega_i), \end{cases}, \qquad \pi_p = \{(i,j),(i',j')\}, \tag{15}$$

form the global skeleton space

$$S_{\mathcal{N}_{\mathcal{P}}} := \{\Psi_{p,k}, \quad 1 \le k \le \mathcal{N}_{\mathcal{P}}, 1 \le p \le P^\Gamma\}. \tag{16}$$

Next, we introduce for each instantiated component i, $1 \le i \le I$ a source bubble $\hat{b}_i^f(\mu_i) \in \hat{B}^{\mathcal{N}}$, defined as the solution of

$$\hat{a}(\hat{b}_i^f(\mu_i), w; \mu_i) = \hat{f}(w; \mu_i), \qquad \forall w \in \hat{B}^{\mathcal{N}}, \tag{17}$$

and set $b_i^f(\mu_i) \equiv \mathcal{T}_i^{map}(\hat{b}_i^f(\mu_i) \circ \mathcal{T}_i^{-1})$. Note that the source bubble $\hat{b}_i^f(\mu_i)$ depends on μ_i, $i = 1, ..., I$ rather than the parameter $\hat{\mu}$ on the archetype component. Additionally we define bubbles $\hat{b}_{i,j,k}(\mu_i) \in \hat{B}^{\mathcal{N}}$ associated with the coupling modes $\hat{\psi}_{j,k}$ as the solutions of

$$\hat{a}(\hat{b}_{i,j,k}(\mu_i) + \hat{\psi}_{j,k}, w; \mu_i) = 0, \qquad \forall w \in \hat{B}^{\mathcal{N}}. \tag{18}$$

Setting $\hat{\phi}_{i,j,k}(\mu_i) \equiv \hat{b}_{i,j,k}(\mu_i) + \hat{\psi}_{j,k}$ and $\phi_{i,j,k}(\mu_i) \equiv \mathcal{T}_i^{map}(\hat{\phi}_{i,j,k}(\mu_i) \circ \mathcal{T}_i^{-1})$, we may introduce the global functions $\Phi_{p,k}(\mu) \in X^{\mathcal{N}}$ as

$$\Phi_{p,k}(\mu) := \begin{cases} \phi_{i',j',k}(\mu_i), & \text{in } \Omega_{i'}, \\ \phi_{i,j,k}(\mu_i), & \text{in } \Omega_i, \\ 0, & \text{in } \Omega \setminus (\Omega_{i'} \cup \Omega_i), \end{cases}, \qquad \pi_p = \{(i,j),(i',j')\}. \tag{19}$$

We highlight that we have $X^{\mathcal{N}} = S_{\mathcal{N}_{\mathcal{P}}} \oplus B^{\mathcal{N}}$. The key result is that thanks to the definition of the coupling modes (14) the decomposition

$$\hat{X}^{\mathcal{N}} = \hat{B}^{\mathcal{N}} \oplus \text{span}\{\hat{\psi}_{j,k},\ \ j = 1, ..., P^\gamma, k = 1, ..., \mathcal{N}_{\mathcal{P}}\}, \quad i = 1, ..., I \tag{20}$$

is $\hat{X}$-orthogonal. Note that we may also employ a parameter independent bilinear form $a(\cdot,\cdot) : \hat{X} \times \hat{X} \to \mathbb{R}$ in (14) as in domain decomposition methods [25] or the CMS approach [4, 5]. However, we emphasize that unlike in standard domain decomposition methods and the CMS approach, where the shape of the component does not vary, the decomposition on the global system $X^{\mathcal{N}} = S_{\mathcal{N}_\mathcal{P}} \oplus B^{\mathcal{N}}$ is in general not orthogonal due to the parameter dependency of the geometric transformation $\mathcal{T}_i$. Note to this end that in contrast to the bilinear form in (18) the inner product in (14) does not depend on geometric parameters.

Finally, we introduce for each instantiated component a global function

$$u_i(\mu) = \begin{cases} \sum_{i=1}^{I} b_i^f(\mu_i) + \sum_{j=1}^{P^\gamma} \sum_{k=1}^{\mathcal{N}_\mathcal{P}} U_{\Pi_i(j),k}(\mu)\phi_{i,j,k}(\mu_i), & \text{in } \Omega_i, \\ 0, & \text{in } \Omega \setminus \Omega_i, \end{cases} \tag{21}$$

with unknown coefficient $U_{\Pi_i(j),k}(\mu) \in \mathbb{R}$. We write

$$u(\mu) = \sum_{i=1}^{I} u_i(\mu_i) = \sum_{i=1}^{I} b_i^f(\mu_i) + \sum_{p=1}^{P^\Gamma} \sum_{k=1}^{\mathcal{N}_\mathcal{P}} U_{p,k}(\mu)\Phi_{p,k}(\mu) \tag{22}$$

and consider

$$\text{For any } \mu \in \mathcal{D}, \text{ find } u(\mu) \in X^{\mathcal{N}} : \; a(u(\mu), v; \mu) = f(v; \mu), \quad \forall v \in S_{\mathcal{N}_\mathcal{P}}. \tag{23}$$

Note that thanks to (17) and (18) problem (23) is equivalent to (12).

3. Model reduction

As the static condensation procedure described in §2 is computationally very expensive we apply model reduction techniques. Within the component interior we construct as in the SCRBE method [14] a reduced basis (RB) approximation [7] for each interface and source bubble (§3.1). Additionally we construct a low-dimensional port space by a pairwise training algorithm [15] and a subsequent proper orthogonal decomposition (POD), which is then used to define a port reduced SCRBE (PR-SCRBE) approximation (§3.2). We prove that the PR-SCRBE and hence the SCRBE approximate problem are well-posed and that the approximation is stable, which is one new contribution of this paper.

3.1. Static condensation reduced basis element method (SCRBE)

For each instantiated component we define the RB approximations $\hat{b}_i^{f;N}(\mu_i) \in \hat{B}_f^N \subset \hat{B}^{\mathcal{N}}$ and $\hat{b}_{i,j,k}^N(\mu_i) \in \hat{B}_{j,k}^N \subset \hat{B}^{\mathcal{N}}$ as the solutions of

$$\hat{a}(\hat{b}_i^{f;N}(\mu_i), w; \mu_i) = \hat{f}(w; \mu_i), \qquad \forall w \in \hat{B}_f^N, \tag{24}$$

$$\hat{a}(\hat{b}_{i,j,k}^N(\mu_i) + \hat{\psi}_{j,k}, w; \mu_i) = 0, \qquad \forall w \in \hat{B}_{j,k}^N, \tag{25}$$

for $1 \le i \le I$ and $1 \le j \le P^\gamma$, $1 \le k \le \mathcal{N}_\mathcal{P}$. Hence each RB approximation $\hat{b}_i^{f;N}(\mu_i)$ and $\hat{b}_{i,j,k}^N(\mu_i)$ is associated with a different RB space $\hat{B}_f^N$ or $\hat{B}_{j,k}^N$ of dimension $\le N$ tailored to the respective bubble, where $N = 1, ..., N_{max}$. Constructing these RB spaces with a Greedy algorithm [26] ensures a rapid convergence of the RB approximation [8]. For further details on RB methods we refer to [7]. We also define $b_i^{f;N}(\mu_i) \equiv \mathcal{T}_i^{map}(\hat{b}_i^{f;N}(\mu_i) \circ \mathcal{T}_i^{-1})$ and

$$b^{f;N}(\mu) := \sum_{i=1}^{I} b_i^{f;N}(\mu_i), \tag{26}$$

where we extend $b_i^{f;N}(\mu_i)$ by zero to $\Omega_{i'}$ for $i' \neq i$. Setting $\hat{\phi}_{i,j,k}^N(\mu_i) \equiv \hat{b}_{i,j,k}^N(\mu_i) + \hat{\psi}_{j,k}$ and $\phi_{i,j,k}^N(\mu_i) \equiv \mathcal{T}_i^{map}(\hat{\phi}_{i,j,k}^N(\mu_i) \circ \mathcal{T}_i^{-1})$, we may introduce the global functions $\Phi_{p,k}^N(\mu) \in X^{\mathcal{N}}$ as

$$\Phi_{p,k}^N(\mu) := \begin{cases} \phi_{i',j',k}^N(\mu_i), & \text{in } \Omega_{i'}, \\ \phi_{i,j,k}^N(\mu_i), & \text{in } \Omega_i, \\ 0, & \text{in } \Omega \setminus (\Omega_{i'} \cup \Omega_i), \end{cases}, \qquad \pi_p = \{(i,j),(i',j')\} \tag{27}$$

and define the SCRBE approximation space $X^N(\mu)$ as

$$X^N(\mu) := \text{span}\{\Phi_{p,k}^N(\mu) : 1 \leq p \leq P^\Gamma, \ 1 \leq k \leq \mathcal{N}_\mathcal{P}\}. \tag{28}$$

We may then consider the problem

$$\text{Find } \tilde{u}_G^N(\mu) \in X^N(\mu) : a(\tilde{u}_G^N(\mu), v; \mu) = f(v;\mu) - a(b^{f;N}(\mu), v; \mu), \quad \forall v \in X^N(\mu), \tag{29}$$

and define an SCRBE approximation $u_G^N(\mu)$ as

$$u_G^N(\mu) = \tilde{u}_G^N(\mu) + b^{f;N}(\mu). \tag{30}$$

Here the index G indicates that we consider a (standard) Galerkin approximation, i.e. that we employ $X^N(\mu)$ both as a test and a trial space.

Alternatively we may perform a Petrov-Galerkin approximation and consider

$$\text{Find } \tilde{u}_{PG}^N(\mu) \in X^N(\mu) : a(\tilde{u}_{PG}^N(\mu), v; \mu) = f(v;\mu) - a(b^{f;N}(\mu), v; \mu), \quad \forall v \in S_{\mathcal{N}_\mathcal{P}}. \tag{31}$$

Then we define the corresponding SCRBE approximation $u_{PG}^N(\mu)$ as

$$u_{PG}^N(\mu) = \tilde{u}_{PG}^N(\mu) + b^{f;N}(\mu). \tag{32}$$

We emphasize that due to the RB approximation the problems (29) and (31) are not equivalent.

3.2. Port reduction

Next we consider reduced port spaces [15, 18] of dimension $n \leq \mathcal{N}_\mathcal{P}$. Note that in general the dimension of the reduced port spaces may vary within the global system even for the same port type. However, for the sake of simplicity and readability we assume that all reduced port spaces within the system have the same dimension n. To obtain a fast convergence of the port reduced approximation and hence an accurate approximation also for $n \ll \mathcal{N}_\mathcal{P}$ we employ empirical port modes, constructed with model reduction techniques related to RB methods [15, 18]. The key idea of the empirical port mode strategy proposed in [15] is to include knowledge on the solution manifold on the port into the basis construction process to obtain a fast converging port reduction approximation. It is exploited that the behavior of the solution on an interior port Γ_p is fully determined by the geometric form, the considered PDE, the parameter values and the behavior of the solution on the non-shared ports of the two components which connect at Γ_p. The purpose of the pairwise training algorithm proposed in [15] for the construction of empirical port modes is thus to explore the solution manifold induced by the parameter dependency regarding geometric and material parameters and an introduced parametrization of the unknown solution behavior on non-shared ports in a systematic fashion to prepare the port modes for all possible component connectivities and parameter configurations that may be encountered in the online stage. For further details we refer to [15, 18].

Now we present the general port reduction framework as introduced in [15] and prove well-posedness of the

PR-SCRBE approximate problem.
First, we introduce a port-reduced skeleton space

$$S_n := \{\Psi_{p,k}, \quad 1 \le k \le n, \;\; 1 \le p \le P^\Gamma\} \subset S_{\mathcal{N}_\mathcal{P}}, \quad \text{with} \quad n \le \mathcal{N}_\mathcal{P}. \tag{33}$$

Furthermore, we introduce a port-reduced SCRBE approximation space

$$X_n^N(\mu) := \text{span}\{\Phi_{p,k}^N(\mu) : \; 1 \le k \le n, \;\; 1 \le p \le P^\Gamma\}, \quad \text{with} \quad n \le \mathcal{N}_\mathcal{P}, \tag{34}$$

and consider the problem

$$\text{Find } \; \tilde{u}_{n,G}^N(\mu) \in X_n^N(\mu) : a(\tilde{u}_{n,G}^N(\mu), v; \mu) = f(v;\mu) - a(b^{f;N}(\mu), v; \mu), \quad \forall v \in X_n^N(\mu). \tag{35}$$

We may then define the Galerkin-PR-SCRBE approximation as

$$u_{n,G}^N(\mu) = b^{f;N}(\mu) + \tilde{u}_{n,G}^N(\mu) = b^{f;N}(\mu) + \sum_{p=1}^{P^\Gamma} \sum_{k=1}^{n} U_{n,G,p,k}^N(\mu) \Phi_{p,k}^N(\mu), \tag{36}$$

where $\tilde{u}_n^N(\mu) = \sum_{p=1}^{P^\Gamma} \sum_{k=1}^{n} U_{n,G,p,k}^N(\mu) \Phi_{p,k}^N(\mu)$ and $U_{n,G,p,k}^N(\mu) \in \mathbb{R}$ denote the coefficients obtained by solving (35).

Lemma 3.1 (Well-posedness of the Galerkin-PR-SCRBE problem (35))**.** *The Galerkin-PR-SCRBE problem* (35) *is well-posed. Moreover, for all* $\mu \in \mathcal{D}$ *and* $f(\mu) \in X^{'}$ *there holds the stability estimate*

$$\|u_{n,G}^N(\mu)\|_X \le \frac{1}{\alpha^\mathcal{N}(\mu)} \left(2 + \frac{\nu^\mathcal{N}(\mu)}{\alpha^\mathcal{N}(\mu)}\right) \|f(\mu)\|_{X'}. \tag{37}$$

Proof. Thanks to our assumption that $a(\cdot,\cdot;\mu)$ is coercive on X with respect to the norm $\|\cdot\|_X$, the RB approximate problems (24) and (25) are well-posed. The mapping from a system parameter $\mu \in \mathcal{D}$ to the space $X_n^N(\mu)$ is hence well defined. We recall that functions in $X_n^N(\mu)$ are zero on ports where we prescribe Dirichlet boundary conditions because P^Γ denotes the number of global ports on which we do not impose Dirichlet conditions. The port compatibility requirement (5) and the fact that $S_n \subset S_{\mathcal{N}_\mathcal{P}}$ then yield that $X_n^N(\mu) \subset X^\mathcal{N}$ and thus that the PR-SCRBE approximation setting is conformal. Therefore, the bilinear form $a(\cdot,\cdot;\mu)$ is coercive on $X_n^N(\mu)$ with coercivity constant $\alpha^\mathcal{N}(\mu)$ and continuous with continuity constant $\nu^\mathcal{N}(\mu)$. The Lax-Milgram Lemma hence implies well-posedness of (35). Exploiting equation (17), the coercivity of $a(\cdot,\cdot;\mu)$ on $X^\mathcal{N}$, and the definitions of $a(\cdot,\cdot;\mu)$ (6), $f(\cdot;\mu)$ (7), and $b^{f;N}(\mu)$ (26) yields

$$\|b^{f;N}(\mu)\|_X \le \frac{1}{\alpha^\mathcal{N}(\mu)} \|f(\mu)\|_{X'}. \tag{38}$$

The stability estimate then follows by testing with $\tilde{u}_{n,G}^N(\mu)$ in (35). □

Again we may consider the Petrov-Galerkin formulation

$$\text{Find } \; \tilde{u}_{n,PG}^N(\mu) \in X_n^N(\mu) : a(\tilde{u}_{n,PG}^N(\mu), v; \mu) = f(v;\mu) - a(b^{f;N}(\mu), v; \mu), \quad \forall v \in S_n. \tag{39}$$

We may then define the PR-SCRBE approximation as

$$u_{n,PG}^N(\mu) = b^{f;N}(\mu) + \tilde{u}_{n,PG}^N(\mu) = b^{f;N}(\mu) + \sum_{p=1}^{P^\Gamma} \sum_{k=1}^{n} U_{n,PG,p,k}^N(\mu) \Phi_{p,k}^N(\mu), \tag{40}$$

where $\tilde{u}_{n,PG}^N(\mu) = \sum_{p=1}^{P^\Gamma} \sum_{k=1}^{n} U_{n,PG,p,k}^N(\mu) \Phi_{p,k}^N(\mu)$ and $U_{n,PG,p,k}^N(\mu) \in \mathbb{R}$ denote the coefficients obtained by solving (39).

Lemma 3.2 (Well-posedness of the Petrov-Galerkin PR-SCRBE problem (39))**.** *Let us assume that for all $\mu \in \mathcal{D}$ the discrete inf-sup condition*

$$\inf_{w \in X_n^N(\mu)} \sup_{v \in S_n} \frac{a(w,v;\mu)}{\|w\|_X \|v\|_X} =: \beta_n^N(\mu) > 0 \tag{41}$$

is fulfilled. Then the Petrov-Galerkin PR-SCRBE problem (39) *is well-posed. Moreover, for all $\mu \in \mathcal{D}$ and $f(\mu) \in X^{'}$ there holds the stability estimate*

$$\|u_{n,PG}^N(\mu)\|_X \leq \left[\frac{1}{\beta_n^N(\mu)}\left(1 + \frac{\nu^{\mathcal{N}}(\mu)}{\alpha^{\mathcal{N}}(\mu)}\right) + \frac{1}{\alpha^{\mathcal{N}}(\mu)}\right] \|f(\mu)\|_{X'}. \tag{42}$$

Proof. The fact that the spaces $X_n^N(\mu)$ and S_n have the same (finite) dimension together with the Banach-Nečas-Babuška Theorem yield the well-posedness of (39) (cf. [27]). The stability estimate can then be obtained by using the a priori estimate (38) and the discrete inf-sup condition. □

Note that the well-posedness of (29) and (31) follows directly from Lemma 3.1 and Lemma 3.2 by considering $n = \mathcal{N}_{\mathcal{P}}$.

4. Certification framework

The goal of this section is to develop a certification framework for the PR-SCRBE method which provides a rigorous and efficient a posteriori error estimator for the error $\|u(\mu) - u_n^N(\mu)\|_X$. To this end we adopt techniques from the RB framework [7] to define an a posteriori error estimator for the error caused by the RB approximation of the bubble functions in the component interior (§4.1.1). To motivate our proposed concept for an a posteriori error estimator for port reduction we recall that the "truth" FE (static condensation) approximation $u(\mu)$ satisfies a weak flux continuity across global ports; to wit for two components i and i' which connect at a global port Γ_p, $\pi_p = \{(i,j),(i',j')\}$ there holds

$$f_i(\Psi_{p,k};\mu_i) - a_i(u_i(\mu_i),\Psi_{p,k};\mu_i) + f_{i'}(\Psi_{p,k};\mu_{i'}) - a_{i'}(u_{i'}(\mu_{i'}),\Psi_{p,k};\mu_{i'}) = 0, \quad k = 1,...,\mathcal{N}_{\mathcal{P}}. \tag{43}$$

For the port reduced SCRBE approximation we also have weak flux continuity but only with respect to the reduced port space. To measure how well the PR-SCRBE approximation behaves like the truth solution on the ports and thus to quantify the error caused by port reduction we hence compute weak fluxes for the PR-SCRBE approximation on all ports of a component with respect to the full port space and use the jump of those fluxes across ports to define an a posteriori error estimator (§4.1.2). To combine both error estimator contributions we exploit the $\hat{X}$-orthogonality of the bubble and the skeleton space on each archetype reference component (20). We state the main results, namely the a posteriori error estimate and the effectivity results, in Sections 4.1 and 4.2 and collect the respective proofs in §4.4. We employ approximations of the occurring constants in the estimator and discuss in §4.3 how such approximations may be obtained. We emphasize that all results in this section hold true both for the Galerkin (35) and the Petrov-Galerkin formulation (39) of the PR-SCRBE method. Thus we omit the respective indices G and PG in this section and recall that the respective PR-SCRBE approximations have been defined in (36) and (40) as

$$u_n^N(\mu) = b^{f;N}(\mu) + \sum_{p=1}^{P^\Gamma} \sum_{k=1}^{n} U_{n,p,k}^N(\mu) \Phi_{p,k}^N(\mu), \quad \text{for } U_{n,p,k}^N(\mu) \in \mathbb{R}.$$

4.1. Formulation and analysis of a rigorous a posteriori error estimator for PR-SCRBE based on local indicators

4.1.1. An a posteriori error estimator for the RB error

First we consider error contributions due to reduced basis approximations of the bubbles defined in (24) and (25). For each instantiated component i, $1 \leq i \leq I$ and $1 \leq j \leq P^\gamma$, $1 \leq k \leq n$ we define the residuals

$$\begin{aligned} \hat{r}_i^f(\hat{w};\mu_i) &:= \hat{f}(\hat{w};\mu_i) - \hat{a}(\hat{b}_i^{f;N}(\mu_i),\hat{w};\mu_i), \quad \forall \hat{w} \in \hat{B}^{\mathcal{N}}, \\ \text{and } \hat{r}_{i,j,k}(\hat{w};\mu_i) &:= -\hat{a}(\hat{\psi}_{j,k} + \hat{b}_{i,j,k}^N(\mu_i),\hat{w};\mu_i), \quad \forall \hat{w} \in \hat{B}^{\mathcal{N}}. \end{aligned}$$

Furthermore, we introduce the corresponding Riesz representations $\hat{\mathcal{R}}_i^f(\mu_i) \in \hat{B}^{\mathcal{N}}$ and $\hat{\mathcal{R}}_{i,j,k}(\mu_i) \in \hat{B}^{\mathcal{N}}$ as the solutions of

$$\begin{aligned} (\hat{\mathcal{R}}_i^f(\mu_i),\hat{w})_{\hat{X}} &= \hat{r}_i^f(\hat{w};\mu_i), \quad \forall \hat{w} \in \hat{B}^{\mathcal{N}}, \\ (\hat{\mathcal{R}}_{i,j,k}(\mu_i),\hat{w})_{\hat{X}} &= \hat{r}_{i,j,k}(\hat{w};\mu_i), \quad \forall \hat{w} \in \hat{B}^{\mathcal{N}}. \end{aligned} \tag{44}$$

We may now employ these Riesz representations to define an a posteriori error estimator $\Delta^N(\mu)$ for the RB error as

$$\begin{aligned} \Delta^N(\mu) &:= \frac{c_{app}^X c_{2,app}^X}{\alpha_{app}(\mu)} \Big(\sum_{i=1}^I (\Delta_i^N(\mu))^2\Big)^{1/2} \\ \text{with} \quad \Delta_i^N(\mu) &:= g(\|G_i\|)|\det G_i|^{-1/2} \|\hat{\mathcal{R}}_i^f(\mu_i) + \sum_{j=1}^{P^\gamma}\sum_{k=1}^n U_{n,\Pi_i(j),k}^N(\mu)\hat{\mathcal{R}}_{i,j,k}(\mu_i)\|_{\hat{X}}. \end{aligned} \tag{45}$$

We emphasize that the inner product employed in (44) does not depend on (geometric) parameters. Therefore the RB error estimator (45) is based on information on the error on the (archetype) reference domain and not on the mapped domain Ω_i in the global system. Note that this is compliant with the standard RB methodology and error estimator for parameter dependent domains Ω [7]. However, the parameter dependency of Ω_i is reflected by the factor $g(\|G_i\|)|\det G_i|^{-1/2}$, on which we will elaborate below. Note also that due to the fact that we employ a different RB approximation for each bubble associated with a coupling mode (cf. §3.1) we have to consider a linear combination of Riesz representations.
We also propose a second error estimator $\Delta^{N,1}(\mu)$ for the RB-induced error which is computationally more feasible than $\Delta^N(\mu)$ especially in terms of storage (see §5). We define $\Delta^{N,1}(\mu)$ as

$$\begin{aligned} \Delta^{N,1}(\mu) &:= \frac{c_{app}^X c_{2,app}^X}{\alpha_{app}(\mu)} \Big(\sum_{i=1}^I (\Delta_i^{N,1}(\mu))^2\Big)^{1/2} \\ \text{for} \quad \Delta_i^{N,1}(\mu) &:= g(\|G_i\|)|\det G_i|^{-1/2}\Big(\|\hat{\mathcal{R}}_i^f(\mu_i)\|_{\hat{X}} + \sum_{j=1}^{P^\gamma}\sum_{k=1}^n |U_{n,\Pi_i(j),k}^N(\mu)|\|\hat{\mathcal{R}}_{i,j,k}(\mu_i)\|_{\hat{X}}\Big). \end{aligned} \tag{46}$$

We remark that one vital improvement to previous contributions [14, 15] is that both $\Delta^N(\mu)$ and $\Delta^{N,1}(\mu)$ yield an estimator for the X-norm of the error (see Proposition 4.2 and Corollary 4.3) and that their validity does not rely on the quality of the RB approximation. We also highlight that both $\Delta^N(\mu)$ and $\Delta^{N,1}(\mu)$ consist of local indicators allowing for an adaptive, component-wise choice of the bubble spaces.
Regarding the constants in (45) and (46), we note that $\alpha_{app}(\mu)$ is an approximation of $\alpha^{\mathcal{N}}(\mu)$ or $\alpha(\mu)$ and

we set $c^X := \sup_{v\in X^{\mathcal{N}}} \|v\|_{H^1(\Omega)}/\|v\|_X$ and $c_2^X := \sup_{v\in X^{\mathcal{N}}} \|v\|_X/\|v\|_{H^1(\Omega)}$ and denote with c_{app}^X and $c_{2,app}^X$ the respective approximations. We remark that we could alternatively define an a posteriori error estimator for the RB error by omitting both c_{app}^X and $c_{2,app}^X$. However adding those constants improved the overall performance of the PR-SCRBE estimator significantly in our numerical experiments. Finally, we remark that the definition of the function $g : \mathbb{R}^+ \to \mathbb{R}^+$ in $g(\|G_i\|)$ depends on the chosen inner product $(\cdot,\cdot)_{\hat{X}}$. For the $H^1(\widehat{\Omega})^{d_r}$-semi-norm we have for instance $g(\|G_i\|) = \|G_i\|$ and for the full $H^1(\widehat{\Omega})^{d_r}$-norm we obtain $g(\|G_i\|) = \|G_i\| + 1$. For other choices of the inner product $(\cdot,\cdot)_{\hat{X}}$ the precise definition of $g(\|G_i\|)$ follows from straightforward calculations exploiting the transformation theorem.

4.1.2. An a posteriori error estimator for port-reduced approximations based on conservative fluxes

Next, we address the error caused by port reduction. To this end we analyze the jump in the flux of the PR-SCRBE approximation $u_n^N(\mu)$ over the ports. As motivated at the beginning of this section we wish to consider a weak flux and hence propose to use a conservative flux defined according to Hughes et al. [19] as a flux measure. The main result in [19] is that by employing a conservative flux the continuous Galerkin method is locally conservative with respect to subdomains consisting of a union of grid elements. The work is based on earlier results (see for instance [28, 29]) which obtain global conservation in spite of the presence of Dirichlet boundary conditions by post-processing. Note that the conservative flux is a variational approximation of the exact flux over the boundary of the component. We adopt the concept proposed in [19] to the PR-SCRBE setting by defining a conservative flux $H_{n,i}^N(\mu)$ for $1 \le i \le I$ as the solution of

$$(H_{n,i}^N(\mu), v)_{L^2(\Sigma_i)} = f_i(v;\mu) - a_i(u_n^N(\mu), v;\mu), \quad \forall v \in S_{\mathcal{N}_\mathcal{P}}, \tag{47}$$

where $\Sigma_i = \bigcup_{1\le j\le P^\gamma} \gamma_{i,j}$. Note that thanks to our mutual disjoint port assumption and the definition of the coupling modes no post-processing, i.e. computation of a global conservative flux, due to Dirichlet boundary conditions as described in [19] is required. Note also that provided $v|_{\Omega_i} = 1 \in S_{\mathcal{N}_\mathcal{P}}$ we may verify mass conservation and that $H_{n,i}^N(\mu)$ is indeed the conserved total flux along Σ_i. Due to the mutual disjoint port assumption problem (47) decouples over different ports and we may compute the conservative flux separately for each port. Thus we have $H_{n,i}^N(\mu)|_{\gamma_{i,j}} = H_{n,i,j}^N(\mu)$, where the latter is defined as the solution of

$$(H_{n,i,j}^N(\mu), \psi_{i,j,k})_{L^2(\gamma_{i,j})} = f_i(\psi_{i,j,k};\mu) - a_i(u_n^N(\mu), \psi_{i,j,k};\mu), \quad 1 \le j \le P^\gamma, 1 \le k \le \mathcal{N}_\mathcal{P}. \tag{48}$$

We may then define the jump of the conservative flux across a global port Γ_p as

$$[H_n^N]_p(x;\mu) := H_{n,i,j}^N(x;\mu) + H_{n,i',j'}^N(x;\mu), \quad \text{where } \pi_p = \{(i,j),(i',j')\}. \tag{49}$$

If a local port $\gamma_{i,j}$ lies on the part of $\partial\Omega$ where Neumann or Robin boundary conditions are prescribed we set $[H_n^N]_p(x;\mu) := H_{n,i,j}^N(x;\mu)$. Based on that we introduce an a posteriori error estimator for port reduction

$$\Delta_n(\mu) := \frac{c_{app}^t c_{app}^X}{\alpha_{app}(\mu)} \Big(\sum_{p=1}^{P^\Gamma} (\Delta_n^p(\mu))^2\Big)^{1/2} \quad \text{for} \quad \Delta_n^p(\mu) := \|[H_n^N]_p(\mu)\|_{L^2(\Gamma_p)^{d_r}}. \tag{50}$$

Here $c_{app}^t := \max_{i\in I} c_{i,app}^t$ and $c_{i,app}^t$ is an approximation of $c_i^t := \sup_{v\in X^{\mathcal{N}}} \|v\|_{L^2(\Sigma_i)}^2/\|v\|_{H^1(\Omega_i)}^2$ for component i. We also introduce $c^t := \max_{i\in I} c_i^t$.

We highlight that in the spirit of standard residual based a posteriori error estimators for the FEM $\Delta_n(\mu)$ consists of local indicators $\Delta_n^p(\mu)$. Below we show a local effectivity result (see Proposition 4.5) for the local indicators. Hence they may be used within an adaptive PR-SCRBE scheme for an efficient choice of local

port spaces on each global port. Note that this is one new contribution of our proposed error estimator, as the error estimator proposed in [15, 18] is based on a (global) non-conforming version of the Schur complement matrix.
Furthermore, we emphasize that we only compute the flux on the ports of each component and hence avoid the computation of a residual on the full global port space as in the CMS approach [5]. Moreover, thanks to our assumption that $\mathcal{T}_i$, $i = 1, ..., I$ when applied to a port is a rigid body motion, the port modes are $L^2(\gamma_{i,j})$-orthonormal, $i = 1, ..., I$, $j = 1, ..., P^\gamma$, and the computation of the conservative flux reduces in this case to the assembling of the residual. If we allow geometric mappings $\mathcal{T}_i$, $i = 1, ..., I$ that deform the port, the port modes are in general not $L^2(\gamma_{i,j})$-orthonormal anymore, and the computational costs for the computation of $\Delta_n(\mu)$ are therefore higher. The effect on the computational costs are further discussed in Subsection 5.2. Note that by restricting the test space in (47) to a subset of $S_{\mathcal{N}_\mathcal{P}}$ a hierarchical, non-rigorous estimator may be computed at lower cost. As in many cases the coefficients of the truth static condensation FE approximation for the high modes are very small, we expect that also this cheaper, non-rigorous estimator would provide a very good estimate of the error induced by port reduction.

4.1.3. Properties of the decomposition $X^\mathcal{N} = B^\mathcal{N} \oplus S_{\mathcal{N}_p}$

Recall that the RB error estimator (45) is based on the dual norm of weighted residuals with respect to the bubble space $B^\mathcal{N}$ and that the PR error estimator (50) rests upon the jump of the conservative flux using the skeleton space $S_{\mathcal{N}_p}$ as a test space. To derive an a posteriori error estimator for the error $u(\mu) - u_n^N(\mu) \in X^\mathcal{N}$ in the X-norm we thus require estimates of the type $\|\Psi\|_X \leq C_1\|v\|_X$ and $\|b\|_X \leq C_2\|v\|_X$ for all $\Psi \in S_{\mathcal{N}_p}$, $b \in B^\mathcal{N}$ and $\Psi + b = v \in X^\mathcal{N}$. The two essential ingredients to derive such estimates are the decomposition $X^\mathcal{N} = B^\mathcal{N} \oplus S_{\mathcal{N}_p}$ and the fact that the decomposition

$$\hat{X}^\mathcal{N} = \hat{B}^\mathcal{N} \oplus \text{span}\{\hat{\psi}_{j,k},\ \ j = 1, ..., P^\gamma, k = 1, ..., \mathcal{N}_\mathcal{P}\}, \quad i = 1, ..., I \tag{51}$$

is $\hat{X}$-orthogonal (see §2.2 for further details). We collect the results in the following proposition.

Proposition 4.1 (Stability of the decomposition $X^\mathcal{N} = B^\mathcal{N} \oplus S_{\mathcal{N}_p}$)**.** *Under the assumptions of Section 2.1.2 on the mapping $\mathcal{T}_i$ the decomposition $X^\mathcal{N} = B^\mathcal{N} \oplus S_{\mathcal{N}_p}$ is stable in the sense that for all $v \in X^\mathcal{N}$, expressed as $v = \Psi + b$ with $\Psi \in S_{\mathcal{N}_p}$ and $b \in X^\mathcal{N}$ we have*

$$\|\Psi\|_{X_i}^2 + \|b\|_{X_i}^2 \leq 2g(\|G_i\|)^2 g(\|G_i^{-1}\|)^2 \|v\|_{X_i}^2, \quad i = 1, ..., I, \tag{52}$$

for constants $0 < g(\|G_i\|), g(\|G_i^{-1}\|) < \infty$. Moreover, the following estimates hold true

$$\|\Psi\|_{X_i} \leq g(\|G_i\|)g(\|G_i^{-1}\|)\|v\|_{X_i} \quad \textit{and} \quad \|b\|_{X_i} \leq g(\|G_i\|)g(\|G_i^{-1}\|)\|v\|_{X_i}, \quad i = 1, ..., I. \tag{53}$$

If the transformation $\mathcal{T}_i$ admits

$$(\psi_{i,j,k}, b)_{X_i} = 0 \quad \forall b \in B_i^\mathcal{N}, \quad i = 1, ..., I, \tag{54}$$

we have the improved result

$$\|\Psi\|_{X_i}^2 + \|b\|_{X_i}^2 = \|v\|_{X_i}^2, \quad i = 1, ..., I. \tag{55}$$

Note that for instance pure rigid body transformations allow for (54).

4.1.4. An a posteriori error estimator for PR-SCRBE

Based on the results above we may now introduce an a posteriori error estimator $\Delta(\mu)$ for the error caused by the PR-SCRBE approximation as

$$\Delta(\mu) = \Delta_n(\mu) + \Delta^N(\mu). \tag{56}$$

The estimator $\Delta(\mu)$ is a rigorous and robust bound as stated in

Proposition 4.2. *Let the approximations of the constants fulfill* $c^X/\alpha(\mu) \leq c^X_{app}/\alpha_{app}(\mu)$, $c^X_2(\mu) \leq c^X_{2,app}(\mu)$ *and* $c^t \leq c^t_{app}$. *Then the error estimator* $\Delta(\mu) = \Delta_n(\mu) + \Delta^N(\mu)$ *with* $\Delta_n(\mu)$ *and* $\Delta^N(\mu)$ *defined in* (50) *and* (45) *satisfies*

$$\|u(\mu) - u^N_n(\mu)\|_X \leq \Delta(\mu). \tag{57}$$

Based on the second RB error estimator $\Delta^{N,1}(\mu)$ we define a second a posteriori error estimator for the error caused by the PR-SCRBE approximation as

$$\Delta^1(\mu) = \Delta_n(\mu) + \Delta^{N,1}(\mu) \tag{58}$$

for which we obtain the following result.

Corollary 4.3. *Let the approximations of the constants fulfill* $c^X/\alpha(\mu) \leq c^X_{app}/\alpha_{app}(\mu)$, $c^X_2(\mu) \leq c^X_{2,app}(\mu)$ *and* $c^t \leq c^t_{app}$. *Then the error estimator* $\Delta^1(\mu) = \Delta_n(\mu) + \Delta^{N,1}(\mu)$ *with* $\Delta_n(\mu)$ *as in* (50) *and* $\Delta^{N,1}(\mu)$ *as defined in* (46) *satisfies*

$$\|u(\mu) - u^N_n(\mu)\|_X \leq \Delta^1(\mu). \tag{59}$$

Note that the structure of $\Delta(\mu)$ and $\Delta^1(\mu)$ allows us to balance the RB and the PR error contributions. Moreover, if the RB error is small, we may employ only $\Delta_n(\mu)$ as a (non-rigorous) a posteriori error estimator, whose computation reduces in general to the assembling of the residual in (48).

4.2. Analysis of the effectivity

In this subsection we derive bounds for the effectivities of the local indicators $\Delta^N_i(\mu)$ (45) and $\Delta^p_n(\mu)$ (50). Based on that we conclude that also the effectivities of $\Delta^N(\mu)$, $\Delta_n(\mu)$, and thus $\Delta(\mu)$ are bounded. First, we study the effectivity of $\Delta^N(\mu)$, i.e. we consider

$$\eta^N(\mu) := \Delta^N(\mu)/\|u(\mu) - u^N_n(\mu)\|_X, \tag{60}$$

and obtain the following result.

Proposition 4.4 (Effectivity of $\Delta^N(\mu)$)**.** *The local error indicators* $\Delta^N_i(\mu)$ *satisfy*

$$\Delta^N_i(\mu) \leq \nu^{\mathcal{N}}(\mu) g(\|G_i\|) g(\|G_i^{-1}\|) \|u(\mu) - u^N_n(\mu)\|_{X_i}. \tag{61}$$

As a result we obtain the following bound for the effectivity $\eta^N(\mu)$

$$\eta^N(\mu) \leq \frac{\nu^{\mathcal{N}}(\mu)}{\alpha_{app}(\mu)} c^X_{app} c^X_{2,app} \max_{i=1,\dots,I} g(\|G_i\|) g(\|G_i^{-1}\|). \tag{62}$$

We recall that we may omit $c^X_{app} c^X_{2,app}$. Thus if $\mathcal{T}_i$, $i = 1, ..., I$, is only a composition of a translation and a rotation and hence $\|G_i\| = \|G_i^{-1}\| = 1$ we recover the standard effectivity result for the RB error estimator based on the dual norm of the residual [7]. Note also that against the background of Proposition 4.1 the constant depending on G_i in (62) reflects how much the geometrical transformation affects the decomposition $X^{\mathcal{N}} = B^{\mathcal{N}} \oplus S_{\mathcal{N}_p}$ in terms of a deviation from orthogonality.

We remark that we cannot obtain an effectivity result for $\Delta^{N,1}(\mu)$.

As a second step we derive a bound for the effectivity of $\Delta_n(\mu)$

$$\eta_n(\mu) := \Delta_n(\mu)/\|u(\mu) - u_n^N(\mu)\|_X, \tag{63}$$

as demonstrated in the following proposition.

Proposition 4.5. *We obtain for the local error indicators $\Delta_n^p(\mu)$ that*

$$\Delta_n^p(\mu) \le \nu^{\mathcal{N}}(\mu) c_h h^{-1/2} C_p(\mu) \|u(\mu) - u_n^N(\mu)\|_{X_i \oplus X_{i'}}, \quad \textit{for } \pi_p = \{(i,j),(i',j')\}, \tag{64}$$

where $\|v\|_{X_i \oplus X_{i'}} := (\|v\|_{X_i}^2 + \|v\|_{X_{i'}}^2)^{1/2}$, $C_p(\mu) := c_{t',i} g(\|G_i^{-1}\|) |\det G_i|^{1/2} + c_{t',i'} g(\|G_{i'}^{-1}\|) |\det G_{i'}|^{1/2}$, $c_{t',i'}$ is the constant in the trace theorem, h denotes the mesh size of the port mesh, and c_h is the constant in the inverse estimate $\|v\|_{H^{1/2}(\Gamma_p)^{d_r}} \le c_h h^{-1/2} \|v\|_{L^2(\Gamma_p)^{d_r}}$ [30] for $v \in \Lambda_{i,j}^{\mathcal{N}_p}$. Moreover, the effectivity $\eta_n(\mu)$ satisfies

$$\eta_n(\mu) \le \frac{\nu^{\mathcal{N}}(\mu)}{\alpha_{app}(\mu)} c_{app}^t c_{app}^X \sqrt{P^\gamma} c_h h^{-1/2} \max_{p=1,\ldots,P^\Gamma} C_p(\mu). \tag{65}$$

We emphasize that in actual practice the dependence of $\eta_n(\mu)$ on h is weak, as will be demonstrated in the numerical experiments in §6. Alternatively we may consider $H^{1/2}$-orthonormal port modes, obtained by a lifting procedure and a corresponding conservative flux expressed as a linear combination of these modes. In this way we can derive a bound for the effectivity $\eta_n(\mu)$ which is independent of the underlying finite element discretization. For further details on the definition and computation of $H^{1/2}$-orthonormal port modes we refer to Appendix A.

Finally we introduce the effectivities of $\Delta(\mu)$ and $\Delta^1(\mu)$

$$\eta(\mu) := \Delta(\mu)/\|u(\mu) - u_n^N(\mu)\|_X \quad \text{and} \quad \eta^1(\mu) := \Delta^1(\mu)/\|u(\mu) - u_n^N(\mu)\|_X \tag{66}$$

and remark:

Corollary 4.6 (Effectivity of $\Delta(\mu)$)**.** *The effectivity $\eta(\mu)$ can be bounded as follows:*

$$\eta(\mu) \le \frac{\nu^{\mathcal{N}}(\mu)}{\alpha_{app}(\mu)} c_{app}^X \left(c_{2,app}^X \max_{i=1,\ldots,I} g(\|G_i\|) g(\|G_i^{-1}\|) + c_{app}^t \sqrt{P^\gamma} c_h h^{-1/2} \max_{p=1,\ldots,P^\Gamma} C_p(\mu) \right). \tag{67}$$

Proof. The bound (67) is a direct consequence of the definition of $\Delta(\mu)$ (56), Proposition 4.4 and Proposition 4.5. □

4.3. Estimation of constants

This subsection is devoted to the discussion of various possibilities to determine approximating constants $\alpha_{app}(\mu)$, c_{app}^t, c_{app}^X and $c_{2,app}^X$ of the constants in the a posteriori error estimators $\Delta(\mu)$ and $\Delta^1(\mu)$.
In some cases a lower bound for $\alpha(\mu)$ and thus $\alpha^{\mathcal{N}}(\mu)$ can be derived analytically as for instance for heat conduction problems. In general we propose to use $\alpha_n^N(\mu) = \inf_{v \in X_n^N(\mu)} a(v,v;\mu)/\|v\|_X^2$ which may be determined by computing for a given parameter $\mu \in \mathcal{D}$ the smallest eigenvalue of the eigenvalue problem: Find the set of eigenvalues and eigenvectors $(\lambda_n^N(\mu), v_n^N(\mu))$, where $\lambda_n^N(\mu) \in \mathbb{R}^+$ and $v_n^N(\mu) \in X_n^N(\mu)$ satisfy

$$a(v_n^N(\mu), w; \mu) = \lambda_n^N(\mu)(v_n^N(\mu), w; \mu)_X \quad \forall w \in X_n^N(\mu). \tag{68}$$

As the left hand side in (68) yields the Schur complement matrix, this requires the assembling of the inner product on the right hand side and the solution of the eigenvalue problem (68). Alternatively we may compute the smallest eigenvalue of the Schur complement matrix which we expect to be a good approximation (but not necessarily a lower bound) of $\alpha_n^N(\mu)$ thanks to the minimax principle.
It remains to justify the choice $\alpha_{app}(\mu) = \alpha_n^N(\mu)$. Note that the derivation of a rigorous lower bound of $\alpha^{\mathcal{N}}(\mu)$ is beyond the scope of this paper. However, we expect $\alpha_n^N(\mu)$ to be a good approximation of $\alpha^{\mathcal{N}}(\mu)$ for the following reasons. We denote by A and M the matrices associated with the left and right hand sides of the "truth" eigenvalue problem: For given $\mu \in \mathcal{D}$ find $(\lambda^{\mathcal{N}}(\mu), v(\mu))$, such that $\lambda^{\mathcal{N}}(\mu) \in \mathbb{R}^+$ and $v(\mu) \in X^{\mathcal{N}}$ satisfy $a(v(\mu), w; \mu) = \lambda^{\mathcal{N}}(\mu)(v(\mu), w)_X$ for all $w \in X^{\mathcal{N}}$. Moreover the subindices P and i refer to the degrees of freedom associated with the ports in the system and the interior of component i, respectively. Exploiting the decomposition $X^{\mathcal{N}} = \mathcal{S}_{\mathcal{N}_\mathcal{P}} \oplus B^{\mathcal{N}}$ and suppressing the dependency of μ, the Schur complement system for the "truth" eigenvalue problem for the smallest eigenvalue $\lambda_1^{\mathcal{N}}(\mu) = \alpha^{\mathcal{N}}(\mu)$ then reads [31]: Find $(\lambda_1^{\mathcal{N}}(\mu), \mathbf{u}_P(\mu)) \in \mathbb{R}^+ \times \mathbb{R}^P$ such that

$$\begin{aligned} &S(\lambda_1^{\mathcal{N}})\mathbf{u}_P(\mu) = \mathbf{0}, \qquad \text{where} \\ &S(\lambda_1^{\mathcal{N}}) = (A_{PP} - \lambda_1^{\mathcal{N}} M_{PP}) - \sum_{i=1}^{I} \left[(A_{iP}^T - \lambda_1^{\mathcal{N}} M_{iP}^T)(A_{ii} - \lambda_1^{\mathcal{N}} M_{ii})^{-1}(A_{iP} - \lambda_1^{\mathcal{N}} M_{iP}) \right], \end{aligned} \tag{69}$$

where $\mathbf{u}_P(\mu)$ denotes the coefficients of the $P = P^\Gamma \mathcal{N}_\mathcal{P}$ degrees of freedom on the ports in the whole system. We observe that $(A_{ii} - \lambda_1^{\mathcal{N}} M_{ii})^{-1}(A_{iP} - \lambda_1^{\mathcal{N}} M_{iP})$ corresponds to the component-local problems: For given $(\mu_i, \sigma) \in \mathcal{D}_i \times [0, \hat{\alpha}_i^{\mathcal{N}}(\mu_i))$ find $\hat{b}_{i,j,k}^\sigma(\mu_i) \in \hat{B}^{\mathcal{N}}$ such that

$$\hat{a}(\hat{b}_{i,j,k}^\sigma(\mu_i), w; \mu_i) - \sigma(\hat{b}_{i,j,k}^\sigma(\mu_i), w; \mu_i)_{\hat{X};\hat{\mu}} = \hat{a}(\hat{\psi}_{j,k}, w; \mu_i) - \sigma(\hat{\psi}_{j,k}, w; \mu_i)_{\hat{X};\hat{\mu}} \qquad \forall w \in \hat{B}^{\mathcal{N}}, \tag{70}$$

for $i = 1, ..., I$, $j = 1, ..., P^\gamma$, $k = 1, ..., \mathcal{N}_\mathcal{P}$. Here $\hat{\alpha}_i^{\mathcal{N}}(\mu_i) := \inf_{\hat{v} \in \hat{B}^{\mathcal{N}}} \hat{a}(\hat{v}, \hat{v}; \mu_i)/\|\hat{v}\|_{\hat{X};\hat{\mu}}^2$ and σ parametrizes the smallest system-level eigenvalue $\lambda_1^{\mathcal{N}}(\mu) = \alpha^{\mathcal{N}}(\mu)$. Note that a similar approach has been proposed in [32]. We emphasize that we request $\sigma \in [0, \hat{\alpha}_i^{\mathcal{N}}(\mu_i))$ and hence $\alpha^{\mathcal{N}}(\mu) < \hat{\alpha}_i^{\mathcal{N}}(\mu_i)$ to obtain well-posedness of (70). Otherwise we define $\alpha_{app}(\mu) := \min_{i=1,...,I} \hat{\alpha}_i^{\mathcal{N}}(\mu_i)$.
Simple calculations yield the estimate

$$(\hat{a}(\hat{b}_{i,j,k}^\sigma(\mu_i) - \hat{b}_{i,j,k}(\mu_i), \hat{b}_{i,j,k}^\sigma(\mu_i) - \hat{b}_{i,j,k}(\mu_i); \mu_i))^{1/2} \leq \sigma(\hat{\alpha_i}^{\mathcal{N}}(\mu_i))^{-1/2} \frac{\hat{\nu}_i^{\mathcal{N}}(\mu_i) + \sigma}{\hat{\alpha_i}^{\mathcal{N}}(\mu_i) - \sigma} \|\hat{\psi}_{j,k}\|_{\hat{X};\hat{\mu}},$$

for $i = 1, ..., I$, $j = 1, ..., P^\gamma$, $k = 1, ..., \mathcal{N}_\mathcal{P}$, $\hat{\nu}_i^{\mathcal{N}}(\mu_i) := \sup_{\hat{v} \in \hat{B}^{\mathcal{N}}} \sup_{\hat{w} \in \hat{B}^{\mathcal{N}}} \hat{a}(\hat{v}, \hat{w}; \mu_i)/\|\hat{v}\|_{\hat{X};\hat{\mu}}\|\hat{w}\|_{\hat{X};\hat{\mu}}$, and $\hat{b}_{i,j,k}(\mu_i)$ as defined in (18). Hence for $\alpha^{\mathcal{N}}(\mu) \ll \hat{\alpha}_i^{\mathcal{N}}(\mu_i)$ we can approximate $S(\lambda_1^{\mathcal{N}})$ in (69) with $S_{app}(\lambda_{1,app}^{\mathcal{N}}) = (A_{PP} - \lambda_{1,app}^{\mathcal{N}} M_{PP}) - \sum_{i=1}^{I} (A_{iP}^T - \lambda_{1,app}^{\mathcal{N}} M_{iP}^T) A_{ii}^{-1} A_{iP}$, which justifies the choice $\alpha_{app}(\mu) = \alpha_n^N(\mu)$ in the case of no RB error and $n = \mathcal{N}_\mathcal{P}$. We emphasize that for problems where $\alpha^{\mathcal{N}}(\mu)$ depends on the geometry of Ω as in the case of linear elasticity we expect $\alpha^{\mathcal{N}}(\mu) \ll \hat{\alpha}_i^{\mathcal{N}}(\mu_i)$, which is verified in the numerical experiments in Section 6.
Thanks to the rapid convergence of the RB approximation [8] we expect also that $\hat{b}_{i,j,k}^N(\mu_i)$ is a good approximation of $\hat{b}_{i,j,k}^\sigma(\mu_i)$. Moreover, due to the expected good approximation behavior of the empirical port modes, demonstrated in Section 6 and [15, 18], we expect a fast convergence of $\alpha_n^N(\mu)$ to the smallest eigenvalue of $S_{app}(\lambda_{1,app}^{\mathcal{N}})$ [31, 33], which finally justifies the usage of $\alpha_n^N(\mu)$ as an approximation of $\alpha^{\mathcal{N}}(\mu)$.

As we apply the trace theorem locally for each instantiated component in the proof of Proposition 4.2 we may exploit the well-known result that the optimal constant c_i^t, $i = 1, .., I$ is the largest eigenvalue of the

generalized eigenvalue problem: Find the set of eigenvalues and eigenvectors $(\lambda(\mu), v(\mu))$, where $\lambda(\mu) \in \mathbb{R}^+$ and $v(\mu) \in X_i^{\mathcal{N}}$ satisfy

$$\begin{aligned}(v(\mu), w)_{L^2(\Sigma_i)} &= ((\mathcal{T}_i^{map})^{-1}(v(\mu)\circ\mathcal{T}_i), (\mathcal{T}_i^{map})^{-1}(w\circ\mathcal{T}_i); \mu_i)_{L^2(\hat{\Sigma})} \\ &= \lambda(\mu)((\mathcal{T}_i^{map})^{-1}(v(\mu)\circ\mathcal{T}_i), (\mathcal{T}_i^{map})^{-1}(w\circ\mathcal{T}_i); \mu_i)_{H^1(\hat{\Omega})} = \lambda(\mu)(v(\mu), w)_{H^1(\Omega_i)} \quad \forall w \in X_i^{\mathcal{N}}.\end{aligned} \tag{71}$$

Note that due to the parameter dependency of the norm standard techniques as the successive constraint method [7] are in general not applicable. In some cases as for simple dilations we can determine analytically for which parameter we obtain an upper bound. For general geometric transformations we propose to solve the eigenvalue problem for the parameter independent norms on the archetype reference component, i.e. we consider: Find the set of eigenvalues and eigenvectors $(\lambda, \hat{v})$, where $\lambda \in \mathbb{R}^+$ and $\hat{v} \in \hat{X}^{\mathcal{N}}$ satisfy

$$(\hat{v}, \hat{w})_{L^2(\hat{\Sigma})} = \lambda(\hat{v}, \hat{w})_{H^1(\hat{\Omega})} \quad \forall \hat{w} \in \hat{X}^{\mathcal{N}}. \tag{72}$$

Then we proceed as in Proposition 4.1 to arrive at the following estimate for the trace constant

$$c_i^t \leq \hat{c}^t(\|G_i\| + 1)|\det G_i|^{-1/2} =: c_{i,app}^t, \tag{73}$$

where $\hat{c}^t$ is the largest eigenvalue of (72). Note, that it is essential to compute a rather sharp bound for c_i^t, $i = 1, ..., I$, as this constant balances the contributions of the RB and PR error estimators.
Finally we address the approximations c_{app}^X and $c_{2,app}^X$, where we focus on the more involved case c_{app}^X. For many PDEs estimating c^X requires the application of Friedrichs inequality. To compute an approximation of the constant in this inequality we propose to proceed as in [34] and decompose Ω in non-overlapping subdomains on which we can derive estimates for the local constants. We use the sharp bound $\mathrm{diam}(\Omega_i)/\pi$ for the constant in Poincaré's inequality for bounded, convex domains Ω_i [35], solve the eigenvalue problem corresponding to Friedrichs inequality on the archetype reference component, and use again Proposition 4.1 to arrive at a bound for the constant in Friedrichs inequality with respect to Ω. For further technical details we refer to [34].

4.4. Proofs

Proof of Proposition 4.1. By expressing $v \in X_i^{\mathcal{N}}$ as $v = \mathcal{T}_i^{map}(\hat{v} \circ \mathcal{T}_i^{-1})$, with $\hat{v} \in \hat{X}^{\mathcal{N}}$ and invoking the transformation theorem we obtain for all $v \in X_i^{\mathcal{N}}$

$$\|v\|_{X_i} \leq g(\|G_i^{-1}\|)|\det G_i|^{1/2}\|\hat{v}\|_{\hat{X}} \quad \text{and} \quad \|\hat{v}\|_{\hat{X}} \leq g(\|G_i\|)|\det G_i|^{-1/2}\|v\|_{X_i}. \tag{74}$$

Then, for $v \in X^{\mathcal{N}}$, expressed as $v = \Psi + b$ with $\Psi \in S_{\mathcal{N}_p}$ and $b \in B^{\mathcal{N}}$, we exploit (74) to obtain

$$\|\Psi\|_{X_i} \leq g(\|G_i^{-1}\|)|\det G_i|^{1/2}\|\hat{\Psi}\|_{\hat{X}} \quad \text{and} \quad \|b\|_{X_i} \leq g(\|G_i^{-1}\|)|\det G_i|^{1/2}\|\hat{b}\|_{\hat{X}}.$$

As $\Psi \in S_{\mathcal{N}_p}$, we may write $\hat{\Psi}$ as a linear combination of the coupling modes $\hat{\psi}_{j,k}$, $i = 1, ..., I$, $j = 1, ..., P^\gamma$, $k = 1, ..., \mathcal{N}_{\mathcal{P}}$. Thanks to (14) also $\hat{\Psi}$ thus fulfills $(\hat{\Psi}, b)_{\hat{X}} = 0$ for all $b \in \hat{B}^{\mathcal{N}}$ which implies

$$\|\hat{\Psi}\|_{\hat{X}}^2 + \|\hat{b}\|_{\hat{X}}^2 = \|\hat{v}\|_{\hat{X}}^2. \tag{75}$$

As a direct consequence we have

$$\|\hat{\Psi}\|_{\hat{X}} \leq \|\hat{v}\|_{\hat{X}} \quad \text{and} \quad \|\hat{b}\|_{\hat{X}} \leq \|\hat{v}\|_{\hat{X}}. \tag{76}$$

Next, we apply again (74) to conclude that

$$\|\Psi\|_{X_i} \leq g(\|G_i^{-1}\|)|\det G_i|^{1/2} g(\|G_i\|)|\det G_i|^{-1/2}\|v\|_{X_i} = g(\|G_i^{-1}\|)g(\|G_i\|)\|v\|_{X_i}$$
$$\text{and} \quad \|b\|_{X_i} \leq g(\|G_i^{-1}\|)g(\|G_i\|)\|v\|_{X_i}.$$

Squaring and summing up yields (52).
Finally, we assume that $\mathcal{T}_i$ admits (54). Expressing Ψ as a linear combination of the mapped coupling modes $\psi_{i,j,k}$, $i = 1, ..., I$, $j = 1, ..., P^\gamma$, $k = 1, ..., \mathcal{N}_\mathcal{P}$ and exploiting (54) yields $(\Psi, b)_{X_i} = 0$ and thus the claim. □

Proof of Proposition 4.2. As $X^\mathcal{N} = B^\mathcal{N} \oplus S_{\mathcal{N}_p}$, we may write each $v \in X^\mathcal{N}$ as $v = b + \Psi$ with $b \in B^\mathcal{N}$ and $\Psi \in S_{\mathcal{N}_p}$. Then we have

$$a(u(\mu) - u_n^N(\mu), v; \mu) = f(v;\mu) - a(u_n^N(\mu), v; \mu) = \underbrace{f(b;\mu) - a(u_n^N(\mu), b; \mu)}_{I:=} + \underbrace{f(\Psi;\mu) - a(u_n^N(\mu), \Psi; \mu)}_{II:=}. \quad (77)$$

For the first part I we invoke the definition of the Riesz representations (44) and the bilinear (6) and linear forms (7) to obtain

$$\begin{aligned} I &= \sum_{i=1}^{I}\big(f_i(b;\mu_i) - a_i(b_i^{f;N}(\mu_i) + \sum_{j=1}^{P^\gamma}\sum_{k=1}^{n} U^N_{n,\Pi_i(j),k}(\mu)\phi^N_{i,j,k}(\mu_i), b; \mu_i)\big) \\ &= \sum_{i=1}^{I}(\hat{\mathcal{R}}_i^f(\mu_i) + \sum_{j=1}^{P^\gamma}\sum_{k=1}^{n} U^N_{n,\Pi_i(j),k}(\mu)\hat{\mathcal{R}}_{i,j,k}(\mu_i), \hat{b})_{\hat{X}} \\ &\leq \sum_{i=1}^{I}\|\hat{\mathcal{R}}_i^f(\mu_i) + \sum_{j=1}^{P^\gamma}\sum_{k=1}^{n} U^N_{n,\Pi_i(j),k}(\mu)\hat{\mathcal{R}}_{i,j,k}(\mu_i)\|_{\hat{X}}\|\hat{b}\|_{\hat{X}}. \end{aligned}$$

Exploiting that functions in $B_i^\mathcal{N}$ vanish on global ports (see (13)) the second part II can be estimated as follows:

$$\begin{aligned} II &= \sum_{i=1}^{I}(H^N_{n,i}(\mu), \Psi)_{L^2(\Sigma_i)^{d_r}} = \sum_{p=1}^{P^\Gamma}([H_n^N]_p(\mu), \Psi)_{L^2(\Gamma_p)^{d_r}} \\ &\leq \big(\sum_{p=1}^{P^\Gamma}\|[H_n^N]_p(\mu)\|^2_{L^2(\Gamma_p)^{d_r}}\big)^{1/2}\big(\sum_{i=1}^{I}\sum_{j=1}^{P^\gamma}\|\Psi\|^2_{L^2(\gamma_{ij})^{d_r}}\big)^{1/2} \\ &= \big(\sum_{p=1}^{P^\Gamma}\|[H_n^N]_p(\mu)\|^2_{L^2(\Gamma_p)^{d_r}}\big)^{1/2}\big(\sum_{i=1}^{I}\sum_{j=1}^{P^\gamma}\|v\|^2_{L^2(\gamma_{ij})^{d_r}}\big)^{1/2} \\ &\leq \big(\sum_{p=1}^{P^\Gamma}\|[H_n^N]_p(\mu)\|^2_{L^2(\Gamma_p)^{d_r}}\big)^{1/2}\big(c_i^t\sum_{i=1}^{I}\|v\|^2_{H^1(\Omega_i)^{d_r}}\big)^{1/2} \leq \big(\sum_{p=1}^{P^\Gamma}\|[H_n^N]_p(\mu)\|^2_{L^2(\Gamma_p)^{d_r}}\big)^{1/2} c^X c^t\|v\|_X. \end{aligned}$$

Proposition 4.1 then leads to

$$\begin{aligned} a(u(\mu) - u_n^N(\mu), v; \mu) \leq c^X\big[c^t\big(\sum_{p=1}^{P^\Gamma}\|[H_n^N]_p(\mu)\|^2_{L^2(\Gamma_p)^{d_r}}\big)^{1/2} \\ + c_2^X\big(\sum_{i=1}^{I} g(\|G_i\|)^2|\det G_i|^{-1}\|\hat{\mathcal{R}}_i^f(\mu_i) + \sum_{j=1}^{P^\gamma}\sum_{k=1}^{n} U^N_{n,\Pi_i(j),k}(\mu)\hat{\mathcal{R}}_{i,j,k}(\mu_i)\|^2_{\hat{X}}\big)^{1/2}\big]\|v\|_X. \end{aligned}$$

Exploiting the coercivity of $a(\cdot,\cdot;\mu)$ with respect to the space $X^{\mathcal{N}}$ yields the claim. □

Proof of Proposition 4.4. For notational convenience we introduce

$$\hat{\mathcal{R}}_i(\mu_i) := \hat{\mathcal{R}}_i^f(\mu_i) + \sum_{j=1}^{P^\gamma}\sum_{k=1}^{n} U^N_{n,\Pi_i(j),k}(\mu)\hat{\mathcal{R}}_{i,j,k}(\mu_i) \in \hat{B}^{\mathcal{N}}$$

and set $\mathcal{R}_i(\mu_i) \equiv \mathcal{T}_i^{map}(\hat{\mathcal{R}}_i(\mu_i)\circ\mathcal{T}_i^{-1})$. Exploiting the definition of $u(\mu)$ in (21),(22), the definition of the bubbles in (17) and (18), and Proposition 4.1 we may estimate on each instantiated component

$$\begin{aligned}
&\|\hat{\mathcal{R}}_i^f(\mu_i) + \sum_{j=1}^{P^\gamma}\sum_{k=1}^{n} U^N_{n,\Pi_i(j),k}(\mu)\hat{\mathcal{R}}_{i,j,k}(\mu_i)\|^2_{\hat{X}}\\
&\quad= f_i(\mathcal{R}_i(\mu_i);\mu_i) - a_i(b_i^{f;N}(\mu_i) + \sum_{j=1}^{P^\gamma}\sum_{k=1}^{n} U^N_{n,\Pi_i(j),k}(\mu)\phi^N_{i,j,k}(\mu_i),\mathcal{R}_i(\mu_i);\mu_i)\\
&\quad= a_i(b_i^f(\mu_i) + \sum_{j=1}^{P^\gamma}\sum_{k=1}^{\mathcal{N}_\mathcal{P}} U_{\Pi_i(j),k}(\mu)\phi_{i,j,k}(\mu_i) - b_i^{f;N}(\mu_i) + \sum_{j=1}^{P^\gamma}\sum_{k=1}^{n} U^N_{n,\Pi_i(j),k}(\mu)\phi^N_{i,j,k}(\mu_i),\mathcal{R}_i(\mu_i);\mu_i)\\
&\quad= a_i(u(\mu)-u_n^N(\mu),\mathcal{R}_i(\mu_i);\mu_i) \le \nu^{\mathcal{N}}(\mu)\|u(\mu)-u_n^N(\mu)\|_{X_i}\|\mathcal{R}_i(\mu_i)\|_{X_i}\\
&\quad\le \nu^{\mathcal{N}}(\mu)\|u(\mu)-u_n^N(\mu)\|_{X_i}\, g(\|G_i^{-1}\|)|\det G_i|^{1/2}\|\hat{\mathcal{R}}_i(\mu_i)\|_{\hat{X}}.
\end{aligned}$$

Squaring and summing up yields the claim. □

Proof of Proposition 4.5. We consider the jump of the conservative flux $[H_n^N]_p(\mu)$ across an arbitrary global port Γ_p, $\pi_p = \{(i,j),(i',j')\}$. Thanks to (49) we may introduce an extension $\mathfrak{R}_p[H_n^N]_p(\mu) = \sum_{k=1}^{\mathcal{N}_p}\varrho_k(\mu)\Psi_{p,k}$ of $[H_n^N]_p(\mu)$ with coefficients $\varrho_k \in \mathbb{R}$. By expressing $\mathfrak{R}_p[H_n^N]_p(\mu)$ as

$$\mathfrak{R}_{\Pi_i(j)}[H_n^N]_{\Pi_i(j)}(\mu) = \mathcal{T}_i^{map}(\hat{\mathfrak{R}}_{\Pi_i(j)}[H_n^N]_{\Pi_i(j)}(\mu)\circ\mathcal{T}_i^{-1})$$

on Ω_i, exploiting the weak flux continuity of the "truth" FE solution $u(\mu)$ across global ports and using Proposition 4.1 we obtain

$$\begin{aligned}
&\|[H_n^N]_p(\mu)\|^2_{L^2(\Gamma_p)^{d_r}}\\
&\quad= f_i(\mathfrak{R}_p[H_n^N]_p(\mu);\mu) - a_i(u_n^N(\mu),\mathfrak{R}_p[H_n^N]_p(\mu);\mu) + f_{i'}(\mathfrak{R}_p[H_n^N]_p(\mu);\mu) - a_{i'}(u_n^N(\mu),\mathfrak{R}_p[H_n^N]_p(\mu);\mu)\\
&\quad= a_i(u(\mu)-u_n^N(\mu),\mathfrak{R}_p[H_n^N]_p(\mu);\mu) + a_{i'}(u(\mu)-u_n^N(\mu),\mathfrak{R}_p[H_n^N]_p(\mu);\mu)\\
&\quad\le \nu^{\mathcal{N}}(\mu)\|u(\mu)-u_n^N(\mu)\|_{X_i\oplus X_{i'}}(\|\mathfrak{R}_p[H_n^N]_p(\mu)\|_{X_i} + \|\mathfrak{R}_p[H_n^N]_p(\mu)\|_{X_{i'}})\\
&\quad\le \nu^{\mathcal{N}}(\mu)\|u(\mu)-u_n^N(\mu)\|_{X_i\oplus X_{i'}}(g(\|G_i^{-1}\|)|\det G_i|^{1/2}\|\hat{\mathfrak{R}}_{\Pi_i(j)}[H_n^N]_{\Pi_i(j)}(\mu)\|_{\hat{X}}\\
&\qquad + g(\|G_{i'}^{-1}\|)|\det G_{i'}|^{1/2}\|\hat{\mathfrak{R}}_{\Pi_{i'}(j')}[H_n^N]_{\Pi_{i'}(j')}(\mu)\|_{\hat{X}}).
\end{aligned}$$

As $\mathfrak{R}_p[H_n^N]_p(\mu) \in S_{\mathcal{N}_p}$ me may exploit (14) to obtain that $\hat{\mathfrak{R}}_{\Pi_i(j)}[H_n^N]_{\Pi_i(j)}(\mu)$ is the harmonic extension of $\widehat{[H_n^N]}_{\Pi_i(j)}(\mu)$ on $\widehat{\Omega}$, where $[H_n^N]_{\Pi_i(j)}(\mu) = \mathcal{T}_i^{map}(\widehat{[H_n^N]}_{\Pi_i(j)}(\mu)\circ\mathcal{T}_i^{-1})$. Thus we may apply a trace theorem [36] to obtain :

$$\begin{aligned}
\|[H_n^N]_p(\mu)\|^2_{L^2(\Gamma_p)^{d_r}} \le \nu^{\mathcal{N}}(\mu)\|u(\mu)-u_n^N(\mu)\|_{X_i\oplus X_{i'}}&(c_{t',i}g(\|G_i^{-1}\|)|\det G_i|^{1/2}\|\widehat{[H_n^N]}_{\Pi_i(j)}(\mu)\|_{H^{1/2}(\hat{\gamma}_j)^{d_r}}\\
&+ c_{t',i'}g(\|G_{i'}^{-1}\|)|\det G_{i'}|^{1/2}\|\widehat{[H_n^N]}_{\Pi_{i'}(j')}(\mu)\|_{H^{1/2}(\hat{\gamma}_{j'})^{d_r}}).
\end{aligned}$$

Thanks to our assumption that $\mathcal{T}_i$ when applied to a port is a pure rigid body motion and the port compatibility requirement (5) we can further estimate :

$$\|[H_n^N]_p(\mu)\|^2_{L^2(\Gamma_p)^{d_r}} \leq \nu^{\mathcal{N}}(\mu)\|u(\mu) - u_n^N(\mu)\|_{X_i \oplus X_{i'}} C_p(\mu)\|[H_n^N]_p(\mu)\|_{H^{1/2}(\Gamma_p)^{d_r}},$$

where $C_p(\mu) = c_{t',i} g(\|G_i^{-1}\|)|\det G_i|^{1/2} + c_{t',i'} g(\|G_{i'}^{-1}\|)|\det G_{i'}|^{1/2}$. By applying the inverse estimate $\|v\|_{H^{1/2}(\Gamma_p)^{d_r}} \leq c_h h^{-1/2}\|v\|_{L^2(\Gamma_p)^{d_r}}$ for all $v \in \Lambda_{i,j}^{\mathcal{N}_p}$, $i = 1, ..., I$, $j = 1, ..., P^\gamma$ we obtain

$$\Delta_n^p(\mu) \leq \nu^{\mathcal{N}}(\mu) c_h h^{-1/2} C_p(\mu)\|u(\mu) - u_n^N(\mu)\|_{X_i \oplus X_{i'}}.$$

Summing up yields

$$\sum_{p=1}^{P^\Gamma} \|[H_n^N]_p(\mu)\|^2_{L^2(\Gamma_p)^{d_r}} \leq (\nu^{\mathcal{N}}(\mu) c_h h^{-1/2} C_p(\mu))^2 \sum_{i=1}^{I} P^\gamma \|u(\mu) - u_n^N(\mu)\|^2_{X_i},$$

and thus the claim. □

5. Offline-Online procedure and analysis of the computational costs

5.1. PR-SCRBE approximation

In this subsection we briefly summarize the computational procedure for the PR-SCRBE approximation and refer to [14, 15] for further details.

Offline. First, we perform the pairwise training algorithm as described in [15, 18] and apply a POD to construct the empirical port modes. Next, we compute on each archetype component for the source term and each coupling mode of the full port space the RB bubble approximation by a Greedy algorithm [26]. We remark that this step is potentially rather expensive especially if we have many degrees of freedom on the ports as it requires a couple of truth solves for each RB approximation and hence each port degree of freedom. Note that if we allow ourselves to have only a reduced port space at our disposal in the online stage we may compute merely the RB bubble approximations corresponding to the coupling modes of the reduced port space at possibly much smaller offline computational costs. Independently, we have often "free" parameters as Young's modulus or the heat conduction coefficient in which the solution of (18) scales linearly as the parameters appear outside the whole integral . Furthermore, we do not have to consider parameters reflecting the spatial orientation as discussed in Section 2.1. Besides, the RB construction process is embarrassingly parallel and thus can be performed in general also for the full port space in a couple of CPU hours. Finally, we prepare the online data sets and load them to computer memory.

Online. We employ a graphical user interface to instantiate once I components from the library, assign the parameters, and connect the components at ports to form the global system. We emphasize that we often encounter only $I_{eff} \ll I$ different components in a system, i.e. components instantiated from a different archetype or with a different parameter configuration, for which we have to perform the component-local online computations. For the remaining components we may just copy the required data. Hence the component-local RB approximations can be computed in $\mathcal{O}(I_{eff} P^\gamma n(QN^2 + N^3))$ operations, where we omit the superindices a and f for Q. Subsequently we assemble the component-local Schur complement matrices in $\mathcal{O}(I_{eff}(P^\gamma)^2 n^2 QN^2)$ operations for the Galerkin formulation and $\mathcal{O}(I_{eff}(P^\gamma)^2 n^2 QN)$ operations for the Petrov-Galerkin formulation. Note that the Galerkin formulation requires the storage of the bilinear form evaluated in all possible combinations of RB bubble approximations for each archetype reference component, which can be critical. Finally, we assemble the Schur complement system with a direct stiffness procedure [14, 15] and solve it.

5.2. A posteriori error estimator

To realize an offline-online decomposition of the a posteriori error estimator we adapt the strategy for the standard RB estimator [7] and compute offline on each archetype component the inner products of Riesz representations ($\Delta^N(\mu)$ and $\Delta^{N,1}(\mu)$) or fluxes ($\Delta_n(\mu)$) for all ($\Delta^N(\mu)$) or some ($\Delta^{N,1}(\mu)$ and $\Delta_n(\mu)$) combinations of coupling modes, associated RB basis functions, and affine terms in the bilinear form. Hence for $\Delta_n(\mu)$ we would for instance compute the flux $C^{l,q}_{i,j,k}$ by solving

$$(\mathcal{C}^{l,q}_{i,j,k}, \hat{\psi}_{j,k})_{L^2(\hat{\Sigma})} = \hat{a}^q(\hat{b}^N_{l,i,j,k}, \hat{\psi}_{j,k}), \tag{78}$$

where $\hat{b}^N_{l,i,j,k}$ denotes the lth RB basis function and $j = 1, ..., P^\gamma, k = 1, ..., \mathcal{N}_\mathcal{P}, l \leq N, q = 1, ..., Q^a$. Online we may then compute the local indicators $\Delta^N_i(\mu), \Delta^{N,1}_i(\mu), \Delta^p_n(\mu)$ by forming a linear combination of the precomputed inner products. Alternatively the PR error estimator can be computed online without offline preparations by assembling and solving (48). Next we discuss the offline and online stages for the a posteriori error estimator in detail.

Offline. As indicated at the beginning of this subsection we have to precompute and store the inner product for the Riesz representations for all combinations of coupling modes, corresponding RB approximations, and affine terms in the bilinear form to accomplish an offline-online decomposition of $\Delta^N(\mu)$. Note that the necessary Riesz representations have already been computed (and stored) during the RB space construction as they are required within the greedy algorithm. Hence the additional offline costs are in general smaller than the costs for the construction of the RB bubble approximations. However, as the required storage is significantly larger than the one required for the data sets for the Schur complement system the computation of $\Delta^N(\mu)$ is in general especially feasible for systems of rather moderate RB space dimensions and moderate values of Q and $\mathcal{N}_\mathcal{P}$.
In contrast for the computation of $\Delta^{N,1}(\mu)$ the data sets for each Riesz representative in (44) can be stored separately. Moreover, no additional offline costs arise as the inner products of the required Riesz representations for the affine terms in the bilinear form and the RB basis functions have already been computed during the greedy algorithm.
To realize an offline-online decomposition of $\Delta_n(\mu)$ we first compute the fluxes $C^{l,q}_{i,j,k}$ (78) and also the respective fluxes for the source term. As the right hand side in equation (78) has already been computed during the data set preparation of the Schur complement matrix and the left hand side of (78) is restricted to the ports, those additional offline computational costs are small in comparison to the ones for the PR-SCBRE approximation. To prepare the inner products of the jumps of the conservative fluxes (49) we have to identify groups of two components which may connect within a global system, loop over each pair of local ports within each of these groups, and form the inner products of the various fluxes. We remark that thanks to the port compatibility requirement and the mutual disjoint port assumption only a reduced number of combinations of coupling modes and associated RB basis functions have to be taken into account and that we hence expect the required storage to be comparable with the one required for the data sets for the Schur complement system for the Galerkin formulation.
Finally, we compute the constants $\hat{c}^t$ and solve the eigenvalue problem associated with Friedrichs inequality with negligible additional offline cost.

Online. Also for the computation of the a posteriori error estimators $\Delta(\mu)$ and $\Delta^1(\mu)$ we exploit that typical systems often feature only $I_{eff} \ll I$ instantiated components for which we have to perform the component-local computations. The operation count for the computation of $\Delta^N(\mu)$ and $\Delta_n(\mu)$ is thus $\mathcal{O}(I_{eff}(P^\gamma)^2 n^2 Q^2 N^2)$. Although the operation counts for $\Delta(\mu)$ are therefore higher than the ones for the PR-SCRBE approximation, we expect the actual computational time for the error estimator to be within a

reasonable range as we only need to evaluate the sum over the precomputed inner products. To compute $\Delta^{N,1}(\mu)$ we form the inner products of the Riesz representations (44) in $\mathcal{O}(I_{eff}P^\gamma nQ^2N^2)$ operations and compute the sum in the local indicators $\Delta_i^{N,1}(\mu)$ in $\mathcal{O}(I_{eff}(P^\gamma)^2n^2)$ operations. For moderate values of Q the operation count for $\Delta^{N,1}(\mu)$ is hence comparable to the one for the computation of the PR-SCRBE approximation.
As mentioned at the beginning of this subsection we may alternatively compute $\Delta_n(\mu)$ only online. We assemble the inactive stiffness matrices and right hand side vectors in (48) associated with the coupling modes $\psi_{i,j,k}$, $i = 1, ..., I$, $j = 1, ..., P^\gamma$, $k = n+1, ..., \mathcal{N}_\mathcal{P}$ in $\mathcal{O}(I_{eff}QNP^\gamma n(\mathcal{N}_\mathcal{P} - n))$ operations. Thanks to the $L^2(\gamma_{i,j})$-orthonormality of the port modes the norm of the jump can then be computed in $\mathcal{O}(I_{eff}P^\gamma n(\mathcal{N}_\mathcal{P}-n))$ operations. If we consider port modes that are not $L^2(\gamma_{i,j})$-orthonormal, e.g. due to a geometric mapping that transforms the port, we have to additionally assemble the matrix of the left hand side in (48) which can be realized in $\mathcal{O}(P_{eff}^\gamma \mathcal{N}_\mathcal{P}^2)$ operations. Here, P_{eff}^γ denotes the number of different port shapes within the global system either due to a different port type or a different geometric mapping. Thus, in this case the operation count for computing the norm of the jump adds up to $\mathcal{O}(P_{eff}^\gamma \mathcal{N}_\mathcal{P}^2 + I_{eff}P^\gamma \mathcal{N}_\mathcal{P}^\sigma)$, where σ depends on the employed solver to solve the linear system in (48). Unless we consider a system with a full port space of a great number of degrees of freedom, i.e. $\mathcal{N}_\mathcal{P} \sim QP^\gamma nN$, the online-only strategy for the computation of $\Delta_n(\mu)$ seems to be preferable in both cases. Moreover for $Q(\mathcal{N}_\mathcal{P} - n) \sim N^2$, which is reasonable for many systems, we expect the operation count for the online-only computation of $\Delta_n(\mu)$ for $L^2(\gamma_{i,j})$-orthonormal port modes to be comparable to the one for the computation of the PR-SCRBE approximation.
Finally, we compute the minimal eigenvalue of the Schur complement matrix to determine $\alpha_{app}(\mu)$ and the global constants c_{app}^X and $c_{2,app}^X$, if necessary. The computational costs are small for instance compared to the assembling of the inactive stiffness matrix as we may employ a high tolerance for the solution of the eigenvalue problem and only need to form a sum of the precomputed local constants to determine c_{app}^X and $c_{2,app}^X$. We summarize that the online operation count for the computation of $\Delta^{N,1}(\mu)$, which we have employed for our numerical tests, is thus $\mathcal{O}(I_{eff}(P^\gamma nQ^2N^2 + (P^\gamma)^2n^2 + QNP^\gamma n(\mathcal{N}_\mathcal{P} - n)))$.

6. Numerical Results

In this section we verify both the effectivity of the a posteriori error estimator $\Delta^1(\mu)$ and the local indicators $\Delta_i^{N,1}(\mu)$, $i = 1, ..., I$ and $\Delta_n^p(\mu)$, $p = 1, ..., P^\Gamma$, and demonstrate the applicability of the introduced certification framework by analyzing the computational costs. To factor out the effect of the geometry of the archetype reference component on the theoretical results, we consider a library of one archetype beam component `component 1` as depicted in Fig. 2. First, we consider heat conduction, where we focus on more theoretical related issues as the analysis of the effectivity results. Next, we consider linear elasticity and demonstrate also for this more demanding vector-valued setting that our error estimator is effective and computable at small additional online costs. Our implementation is in C++ and based on the finite element library libMesh [37, 38]. For the solution of the generalized eigenvalue problems we have employed the Krylov–Schur solver of the library SLEPc [39]. For notational convenience we add a subscript or superscript *rel* if we refer to relative error quantities, i.e. quantities divided by $\|u(\mu)\|_X$.

6.1. Heat conduction

We consider equilibrium heat conduction for the beam archetype component `component 1` (see Fig. 2) with heat transfer from the surface of the beam to the ambient for a prescribed uniform heat generation q^{dim}; a combination of a uniform heat flux q_{fl}^{dim} on the bottom of the beam and a volumetric heat generation q_{vol}^{dim}. Such a heat conduction component might be part of a pin heat sink used for instance as a processor cooler.

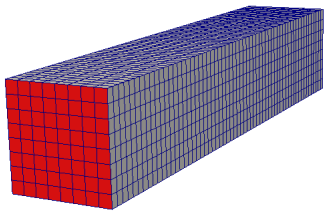

Figure 2: Archetype reference beam component `component 1` with two ports; one at the top and one at the bottom of the beam

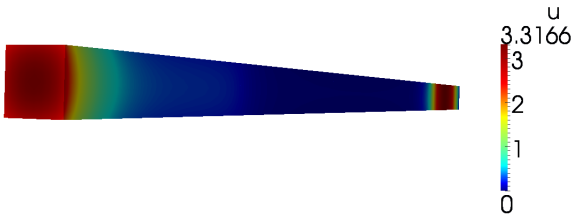

Figure 3: Distribution of the temperature u for `system 1`

First, we nondimensionalize length with respect to a reference length $w^{dim,0}$ and we introduce a non-dimensional conductivity ratio $\kappa = k^{dim}/k^{dim,0}$ for the thermal conductivity k^{dim} and a reference conductivity $k^{dim,0}$. Furthermore we nondimensionalize the heat transfer coefficient h^{dim} with respect to $\kappa\, Bi/(k^{dim,0}w^{dim,0})$ for the dimensionless Biot number $Bi = h^{dim}w^{dim,0}/k^{dim}$, and introduce the non-dimensional temperature $u = k^{dim,0}(T^{dim} - T^{dim}_{ambient})/(q^{dim}(w^{dim,0})^2)$. Finally, we introduce the non-dimensional heat flux $q_{fl} = q^{dim}_{fl}/q^{dim}$ and the non-dimensional volumetric heat generation $q_{vol} = q^{dim}_{vol}/q^{dim}$. On a physical domain $\Omega = (0, 5L) \times (-0.5, 0.5) \times (-0.5, 0.5)$ we may then consider the non-dimensional PDE

$$\begin{aligned} -\kappa\Delta u &= q_{vol} \quad \text{over } \Omega, \\ \kappa\nabla u \cdot n + \kappa Biu &= 0 \quad \text{on } \partial\Omega \setminus (\Gamma_N \cup \Gamma_D), \\ \kappa\nabla u \cdot n &= q_{fl} \quad \text{on } \Gamma_N, \\ u &= 0 \quad \text{on } \Gamma_D, \end{aligned}$$

where L denotes the length scaling and Γ_N and Γ_D the Neumann and the Dirichlet boundary, respectively. We define the following bilinear and linear forms on the archetype reference domain $\widehat{\Omega} = (0, 5) \times (-0.5, 0.5) \times (-0.5, 0.5)$ for the parameter $\hat{\mu} = (\hat{\kappa}, \hat{Bi}, \hat{L}, \hat{q}_{vol}, \hat{q}_{fl})$:

$$\begin{aligned} \hat{a}(\hat{v}, \hat{w}; \hat{\mu}) &:= (\hat{\kappa}/\hat{L}) \int_{\widehat{\Omega}} \frac{d\hat{v}}{d\hat{x}_1}\frac{d\hat{w}}{d\hat{x}_1} + \hat{\kappa}\hat{L} \int_{\widehat{\Omega}} \frac{d\hat{v}}{d\hat{x}_2}\frac{d\hat{w}}{d\hat{x}_2} + \frac{d\hat{v}}{d\hat{x}_3}\frac{d\hat{w}}{d\hat{x}_3} + \hat{Bi}\hat{\kappa}\hat{L} \int_{\partial\widehat{\Omega}\setminus(\hat{\gamma}_1\cup\hat{\gamma}_2)} \hat{v}\hat{w}, \\ \hat{f}(v; \mu) &:= \hat{L} \int_{\widehat{\Omega}} \hat{q}_{vol}\hat{v} + \int_{\hat{\gamma}_2} \hat{q}_{fl}\hat{v}, \end{aligned}$$

where $\hat{\gamma}_1 = \{0\} \times (-0.5, 0.5) \times (-0.5, 0.5)$ and $\hat{\gamma}_2 = \{5\} \times (-0.5, 0.5) \times (-0.5, 0.5)$ are the local ports of the component. We set the parameter space $\hat{\mathcal{D}}$ to $\hat{\mathcal{D}} := [0.5, 2] \times [0.001, 1] \times [0.6, 1.4] \times [-1, 1] \times [-10, 10]$. Note that thanks to the choice of the scale of the Biot number the parameter $\hat{\kappa}$ is a "free" parameter with respect to the RB bubble approximation as it appears in front of the integral in the bilinear form. Finally, we define the inner products

$$\begin{aligned} (\hat{v}, \hat{w})_{\hat{X}} &:= \int_{\widehat{\Omega}} \frac{d\hat{v}}{d\hat{x}_1}\frac{d\hat{w}}{d\hat{x}_1} + \frac{d\hat{v}}{d\hat{x}_2}\frac{d\hat{w}}{d\hat{x}_2} + \frac{d\hat{v}}{d\hat{x}_3}\frac{d\hat{w}}{d\hat{x}_3}, \\ (\hat{v}, \hat{w}; \hat{\mu})_{\hat{X};\hat{\mu}} &:= (1/\hat{L}) \int_{\widehat{\Omega}} \frac{d\hat{v}}{d\hat{x}_1}\frac{d\hat{w}}{d\hat{x}_1} + \hat{L} \int_{\widehat{\Omega}} \frac{d\hat{v}}{d\hat{x}_2}\frac{d\hat{w}}{d\hat{x}_2} + \frac{d\hat{v}}{d\hat{x}_3}\frac{d\hat{w}}{d\hat{x}_3}, \end{aligned} \tag{79}$$

and consider the solution space $X = \{v \in H^1(\Omega) : v = 0 \text{ on } \Gamma_D\}$.
Unless otherwise stated we consider for this test case the Galerkin formulation of the PR-SCRBE method (35). Thus thanks to Lemma 3.1 we obtain well-posedness of the approximation and $\alpha^{\mathcal{N}}(\mu) \geq 0.5 =: \alpha_{app}(\mu)$.

To determine an approximation c^t_{app} for c^t we compute the largest eigenvalue of (71) for $\hat{L} = 0.5$ and obtain $c^t \leq c^t_{app} \approx 1.10464$ for all $\mu \in \mathcal{D}$. Thanks to the definition of the inner products in (79), we have $c^X_2(\mu) \leq 1 =: c^X_{2,app}$. To compute an approximation of c^X, we use the simplified version of the strategy proposed in [34] and obtain $c^X \leq c_F(\mu) \leq \sqrt{(\mathrm{diam}(\Omega)/\pi)^2 + (5IL_i)^2/3} =: c^X_{app}$, where L_i, $i = 1, ..., I$ denotes the length scaling parameter of the i-th instantiated component and $c_F(\mu)$ the constant in the Friedrichs inequality.

Initially we consider a component library `library 1` where we use an underlying FE discretization with $\mathcal{N} = 4941$ linear hexahedral elements and a reference port dimension of $\mathcal{N}_\mathcal{P} = 81$. To generate the empirical port modes we apply the pairwise training algorithm[1] [15, 18], compress the data to 6 POD modes and add the constant mode to obtain 7 empirical port modes. For the RB construction in the offline phase we have set relative tolerance for the Greedy algorithm to 10^{-7}.

First, we consider a `system 1` of $i = 5$ components with component parameters $\mu_1 = (0.5, 0.01, 1.0, 0.5, -)$, $\mu_2 = \mu_3 = \mu_4 = (1.0, 0.5, 1.0, 0.1, -)$, and $\mu_5 = (1.0, 1.0, 1.0, 1.0, 5.0)$. The PR-SCRBE approximation is depicted in Fig. 3 and we observe a rapid temperature drop in component 5 (in the foreground of the picture) because of the relatively high Biot number $Bi = 1.0$.

Analyzing the convergence behavior of the relative error $\|u(\mu) - u^N_n(\mu)\|^{rel}_X$ and the relative error estimator $\Delta^1_{rel}(\mu)$ (58) for $N = N_{max}$ and an increasing number of port modes n in Fig. 4a we observe that $\Delta^1_{rel}(\mu)$ is both a rather sharp and an effective error bound. This also applies if we consider $n = 81$ port modes and hence no port reduction and increase the number of RB basis functions N (cf. Fig. 4d). Next we consider both a reduced number of RB basis functions N and empirical port modes n. We use either $N = 8$ RB basis functions and increase the number of port modes n (cf. Fig. 4b) or choose $n = 6$ and increase N (cf. Fig. 4e). In both cases $\Delta^1(\mu)$ captures the behavior of the respective dominant model error and is able to detect the error plateau due to a too small number of RB basis functions in Fig. 4b or port modes in Fig. 4e. The effectivity changes only very slightly if the type of the dominating model error changes. We hence conclude that for the considered test case $\Delta^1(\mu)$ captures the interaction between the RB and PR error very well and thus may be employed to balance both error contributions during the online phase, which allows us to realize significant computational savings as will be demonstrated below.

If we compare the convergence behavior of the local RB indicators $\Delta^{N,1}_i(\mu_i)$ (46) and the local errors $\|u(\mu) - u^N_n(\mu)\|_{X_i}$ for $i = 1, 4, 5$ in Fig. 4f, we observe that the local effectivities $\Delta^{N,1}_i(\mu_i)/\|u(\mu) - u^N_n(\mu)\|_{X_i}$ change only very slightly for increasing N and that for all considered N the local indicators are able to detect the error distribution on the components. Regarding the local PR indicators $\Delta^p_n(\mu)$ (50), $p = 1, 4, 5$, we observe that the indicators for $p = 1$ and $p = 5$ capture the error behavior of $\|u(\mu) - u^N_n(\mu)\|_{X_1 \oplus X_2}$ and $\|u(\mu) - u^N_n(\mu)\|_{X_5}$ perfectly for increasing n (cf. Fig. 4c). Due to Proposition 4.5 one might expect that the local indicator $\Delta^4_n(\mu)$ behaves as $\|u(\mu) - u^N_n(\mu)\|_{X_4 \oplus X_5}$ for growing n, but instead it shows the same convergence behavior as $\|u(\mu) - u^N_n(\mu)\|_{X_4}$ (cf. Fig. 4c). However, we emphasize that the observed behavior in Fig. 4c is indeed preferable as the error in component 5 is mainly caused by the strong temperature drop near the global (Neumann) port Γ_5 (cf. Fig. 2). To reduce the PR error we should therefore increase the number of port modes at port Γ_5, as suggested by the local indicators $\Delta^4_n(\mu)$ and $\Delta^5_n(\mu)$, and not Γ_4. We remark that similarly also $\Delta^2_n(\mu)$ tends to behave like $\|u(\mu) - u^N_n(\mu)\|_{X_3}$ and not like $\|u(\mu) - u^N_n(\mu)\|_{X_2 \oplus X_3}$. Finally, we note that the local indicators $\Delta^p_n(\mu)$ are able to predict the error distribution on the ports well (cf. Fig. 4c).

Next we consider a `system 2` of 2 components with component parameters $\mu_1 = (1.0, Bi, 1.0, 0.5, -)$ and $\mu_2 = (1.0, Bi, 1.0, 0.5, 5.0)$ and varying Biot number Bi. For $n = 81$ and $N = 10$ we see in Fig. 5a that the local effectivities $\Delta^{N,1}_i(\mu_i)/\|u(\mu) - u^N_n(\mu)\|_{X_i}$ change very little if we increase the Biot number and that for all

[1] Following the notation in [18] we have chosen $N_{\mathrm{samples}} = 500$ and $\gamma = 2$ in the pairwise training algorithm.

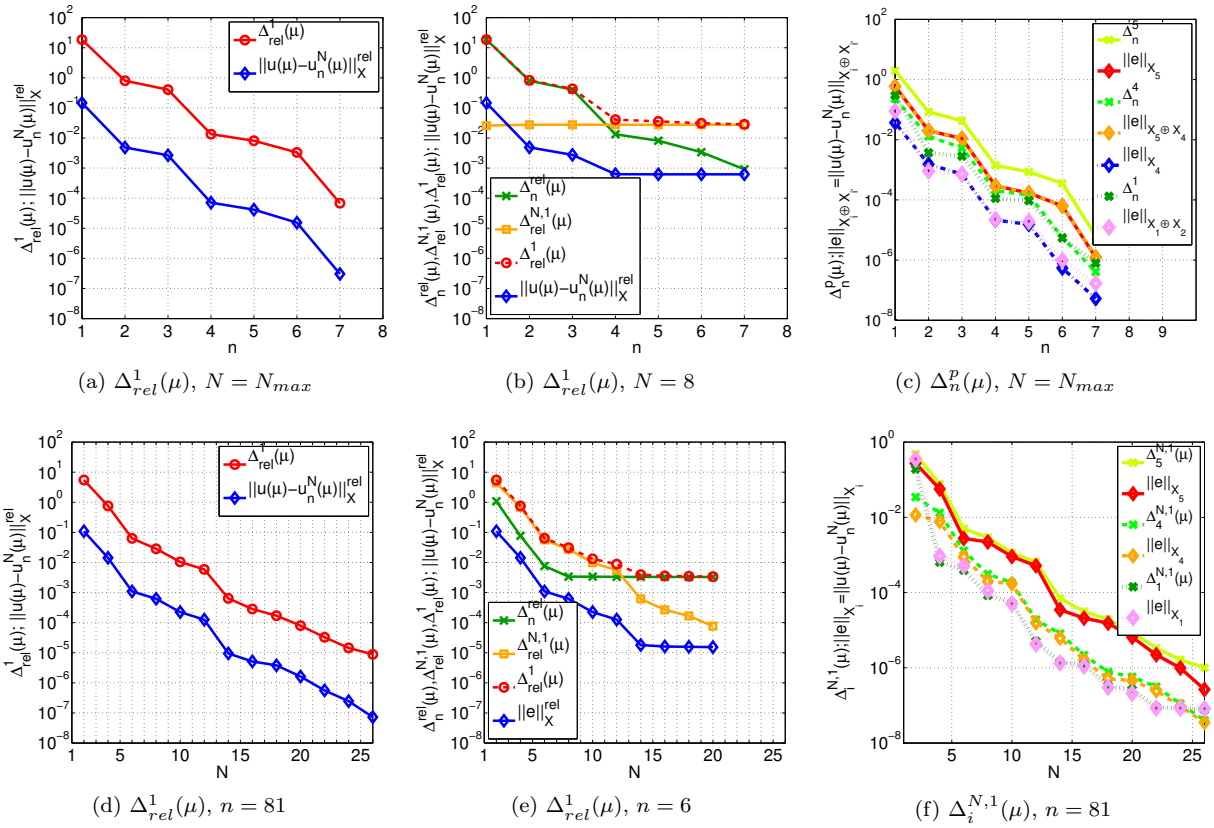

(a) $\Delta^1_{rel}(\mu)$, $N = N_{max}$ (b) $\Delta^1_{rel}(\mu)$, $N = 8$ (c) $\Delta^p_n(\mu)$, $N = N_{max}$

(d) $\Delta^1_{rel}(\mu)$, $n = 81$ (e) $\Delta^1_{rel}(\mu)$, $n = 6$ (f) $\Delta^{N,1}_i(\mu)$, $n = 81$

Figure 4: Behavior of the error estimator $\Delta^1(\mu)$ (58) and the local PR error indicators $\Delta^p_n(\mu)$ (50) on the global port Γ_p and the local RB error indicators $\Delta^{N,1}_i(\mu)$ (46) on component i for `system 1`; $e := u(\mu) - u^N_n(\mu)$.

considered values $Bi \in [0.001, 1]$ the local indicators detect the correct error distribution on the components. If we consider $n = 4$ and $N = N_{max}$ we observe that the local indicator $\Delta^p_2(\mu)$ associated with the Neumann port captures the behavior of $\|u(\mu) - u^N_n(\mu)\|_{X_2}$ very well for varying Bi and that again $\Delta^p_1(\mu)$ tends to behave like $\|u(\mu) - u^N_n(\mu)\|_{X_1}$ rather than $\|u(\mu) - u^N_n(\mu)\|_{X_1 \oplus X_2}$ (cf. Fig. 5b). A possible explanation for the fact that for smaller Biot numbers we have $\Delta^p_1(\mu) \geq \Delta^p_2(\mu)$ might be that in this parameter range the temperature drop is much less localized than for say $Bi = 0.5$ and hence more strongly affects the behavior at port Γ_1.

All in all we thus conclude that for this test case the observed behavior of the local indicators Δ^p_n, $p = 1, ..., P^\Gamma$ confirms the effectivity result of Proposition 4.5 and that the local indicators $\Delta^{N,1}_i(\mu_i)$ capture the local error behavior very well. Moreover the local indicators are able to predict the error distribution on the ports or the components, respectively, relatively well.

To investigate the behavior of the error estimator subject to varying L and hence a non-orthogonal geometric transformation, we consider a `system 3` of 2 components with component parameters $\mu_1 = (1.0, 0.5, L, 0.5, -)$ and $\mu_2 = (1.0, 0.5, L, 0.5, 5.0)$. Note that thanks to the high Biot number the temperature near the Neumann boundary drops very quickly (similar to Fig. 2) and the effect of the length scaling of the beam on the temperature behavior is therefore rather small. Considering this system thus allows us to some extent

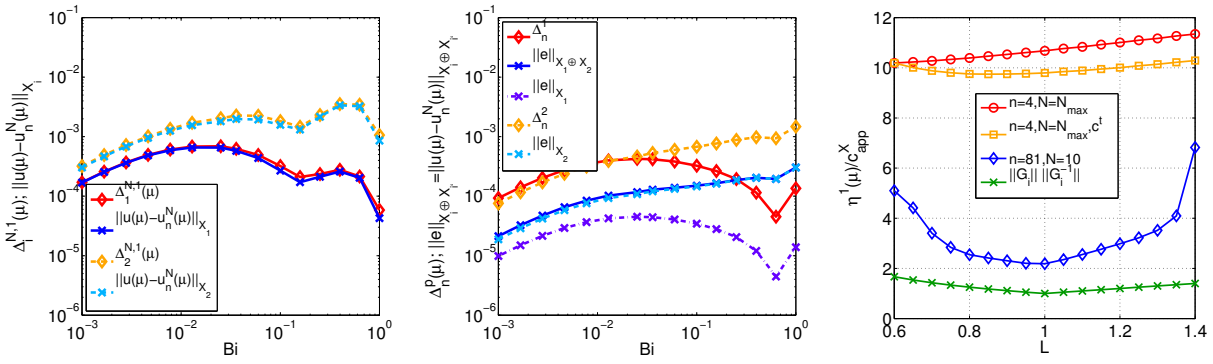

(a) $\Delta_i^{N,1}(\mu)$, $n = 81$ (b) $\Delta_n^p(\mu)$, $N = N_{max}$ (c) $\eta^1(\mu)/c_{app}^X$

Figure 5: Behavior of the local indicators $\Delta_i^{N,1}(\mu)$ (a) and $\Delta_n^p(\mu)$ (b) for `system 2` and varying Biot number; $e := u(\mu) - u_n^N(\mu)$. $\eta^1(\mu)/c_{app}^X$ for `system 3` and varying length scaling parameter L (c).

to analyze the dependency of the error estimator and the effectivities on the constants accounting for the geometric transformation. The results are depicted in Fig. 5c and we observe that for $n = 4$, $N = N_{max}$ the effectivity $\eta^1(\mu)/{c_{app}^X}^2$ slightly grows if we increase L. However if we employ the exact trace constant c^t (Fig. 5c, square markers) the effectivity barely changes, although Proposition 4.5 suggests a dependency on L. Setting $n = 81$, $N = 10$ we see that the effectivity of $\eta^1(\mu)/c_{app}^X$ deteriorates slightly more than anticipated when departing from $L = 1$, but that the deviations are still rather small. We therefore conclude that at least for the considered test case $\Delta^1(\mu)$ seems to be a sharp and effective bound also for systems that include components subject to geometrical non-orthogonal transformations.

Next, we analyze the dependency of $\eta_n(\mu)$ on the port mesh size h. To this end we consider three different libraries of `component 1` with linear hexahedral FE, a fixed mesh size $H = 0.1$ in $\hat{x}_1$-direction, and varying port mesh size $h = 0.2, 0.1, 0.05$ in $\hat{x}_2$- and $\hat{x}_3$-direction in reference coordinates. We have used c_{app}^t associated with the finest mesh. For $h = 0.1$ and $h = 0.05$ we obtained 7 empirical modes and for $h = 0.2$ we obtained 5 empirical modes[3]. The relative tolerance for the Greedy algorithm has been set to 10^{-7}. Moreover, we consider the Petrov-Galerkin formulation (39) for the PR-SCRBE method. We consider a `system 4` of 4 components with parameter configurations $\mu_1 = \mu_2 = \mu_3 = (1.0, 0.25, 1.0, 1.0, -)$ and $\mu_4 = (1.0, 0.5, 1.0, 1.0, 1.0)$ for which we obtain a non-constant temperature distribution on all ports thanks to the moderate Biot number and the high volumetric heat source. The behavior of $\eta_n(\mu)$ for $h/2$ divided by $\eta_n(\mu)$ for h for increasing n is depicted in Fig. 6a and we observe that the ratios are indeed bounded by the expected upper bound $\sqrt{2}$. As we have observed smaller ratios for other systems as for instance for `system 1`, we conclude that it seems like the effectivity $\eta_n(\mu)$ scales in h as anticipated.

Finally, we address the computational costs and consider to this end again `system 1`. We note that thanks to the parameter configuration $\mu_1 = (0.5, 0.01, 1.0, 0.5, -)$, $\mu_2 = \mu_3 = \mu_4 = (1.0, 0.5, 1.0, 0.1, -)$, and $\mu_5 = (1.0, 1.0, 1.0, 1.0, 5.0)$ we obtain $I_{eff} = 3$. First, we compare for $n = 7$ and increasing N the online CPU time for $\Delta_n(\mu)$, $\Delta^{N,1}(\mu)$, and for the PR-SCRBE approximation, i.e. the computation of the RB bubble approximation, the assembly of the Schur complement system and its solution. We observe that the

[2]Note that we divide by c_{app}^X to factor out the effect of the change of c_{app}^X for varying L.

[3]We have set the parameters for the pairwise training algorithm to $N_{samples} = 500$ and $\gamma = 2$.

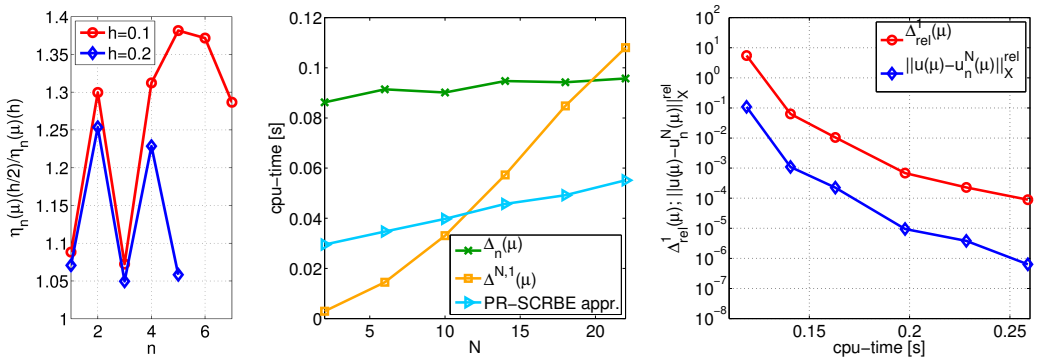

(a) dependence on h (b) CPU time for PR-SCRBE,$\Delta^1(\mu)$ (c) CPU time vs. error, $\Delta^1_{rel}(\mu)$

Figure 6: $\eta_n(\mu)$ for $h/2$ divided by $\eta_n(\mu)$ for h for `system 4` (a). CPU time for the PR-SCRBE approximation and $\Delta^1(\mu)$ for `system 1` and $n = 7$ and increasing N (b) and plot of $\|u(\mu) - u_n^N(\mu)\|_X^{rel}$, $\Delta^1_{rel}(\mu)$ versus the required CPU time for `system 1` for $n = 7$ and increasing N (c).

PR-SCRBE approximation scales linearly in N and that the costs for the computation of $\Delta_n(\mu)$ increase only very slightly from around 0.086 seconds required for $N = 2$ (cf. Fig. 6b). Moreover we see a quadratic scaling of $\Delta^{N,1}(\mu)$ which confirms the operation count in §5. As the CPU time for the computation of $\Delta^1(\mu)$ accounts for about 75% of the online costs we hence infer that the proposed certification framework is indeed computationally feasible and that the error estimator can be computed at a reasonable additional online cost. The computational costs for the corresponding "truth" approximation account on average for 2.25 seconds, where we have employed a conjugate gradient method with a relative tolerance of 10^{-08} both for the solution of the Schur complement system and the linear system of equations for the "truth" FE approximation. Hence for a relative error $\|u(\mu) - u_n^N(\mu)\|_X^{rel}$ of 10^{-06} and an estimated relative error $\Delta^1_{rel}(\mu)$ of 10^{-04} we gain one order of magnitude already for this small considered system (cf. Fig. 6c). Greater computational savings can be realized for larger systems as considered in [18], especially for situations with $I_{eff} \ll I$. We finally note that if we consider $n = 7$ port modes and prescribe (say) a relative error tolerance of 10^{-02} the error estimator indicates that it is sufficient to consider $N = 11$ RB basis functions and we may thus reduce the online costs to around 60% of the online costs that arise for $N = N_{max}$ (cf. Fig. 6c). This demonstrates that we may realize large computational online savings by employing $\Delta^1(\mu)$ to balance the error contributions due to RB and PR model reduction.

6.2. Linear Elasticity

In this test case we consider isotropic linear elasticity for the beam archetype component `component 1` (see Fig. 2). Again, we nondimensionalize length with respect to a reference length $w^{dim,0}$ and we nondimensionalize Young's modulus E^{dim} with respect to a reference value $E^{dim,0}$. We consider a traction $\tau^{dim} \in \mathbb{R}^3$ acting on the tip of the beam, which we nondimensionalize with respect to $E^{dim,0}$, and homogeneous Dirichlet boundary conditions on the bottom of the beam. We do not take into account gravity. We may then introduce the dimensionless displacement $u = u^{dim}/w^{dim,0}$. Finally, we define the non-dimensional tensor $\hat{C}$ as

$$\hat{C}_{ijkl} = \frac{\nu}{(1+\nu)(1-2\nu)}\delta_{ij}\delta_{kl} + \frac{1}{2(1+\nu)}(\delta_{ik}\delta_{jl} + \delta_{il}\delta_{jk}), \quad 1 \le i,j,k,l \le 3,$$

where we choose Poisson's ratio $\nu = 0.3$ for steel.

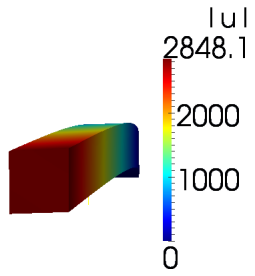

Figure 7: Magnitude of the displacement field u for `system 5`

	$N=1$	$N=2$	$N=3$
Galerkin	$2.942035 \cdot 10^{-03}$	$4.908761 \cdot 10^{-04}$	$2.310078 \cdot 10^{-04}$
Petrov-Galerkin	$3.484242 \cdot 10^{-03}$	$-1.736349 \cdot 10^{-03}$	$2.222161 \cdot 10^{-04}$
	$N=5$	$N=10$	$\alpha^{\mathcal{N}}(\mu)$
Galerkin	$2.307751 \cdot 10^{-04}$	$2.3077506 \cdot 10^{-04}$	$6.905847 \cdot 10^{-04}$
Petrov-Galerkin	$2.306615 \cdot 10^{-04}$	$2.307751 \cdot 10^{-04}$	$6.905847 \cdot 10^{-04}$

Table 1: `system 5`: $\alpha_{app}(\mu)$ for the Galerkin (35) and the Petrov-Galerkin formulation (39) for increasing N.

We consider the archetype parameter vector $\hat{\mu} = (\hat{E}, \hat{L}, \hat{\tau}^2, \hat{\tau}^3)$, where the geometric parameter $\hat{L}$ allows for a length scaling of the archetype reference component domain $\widehat{\Omega} = (0,5) \times (-0.5, 0.5) \times (-0.5, 0.5)$ in the $\hat{x}_1$-direction. Moreover we choose the parameter space $\hat{\mathcal{D}} = [1.0, 10] \times [0.5, 2.0] \times [-1, 1] \times [-1, 1]$. We may then define the following bilinear and linear forms on $\widehat{\Omega}$:

$$\begin{aligned}
\hat{a}(\hat{w}, \hat{v}; \hat{\mu}) &= \hat{E} \left(\int_{\widehat{\Omega}} \frac{\partial \hat{w}^i}{\partial \hat{x}_1} \hat{C}_{i1kl} \frac{\partial \hat{v}^k}{\partial \hat{x}_l} + \int_{\widehat{\Omega}} \frac{\partial \hat{w}^i}{\partial \hat{x}_j} \hat{C}_{ijk1} \frac{\partial \hat{v}^k}{\partial \hat{x}_1} \right) \\
&\quad + \frac{\hat{E}}{\hat{L}} \int_{\widehat{\Omega}} \frac{\partial \hat{w}^i}{\partial \hat{x}_1} \hat{C}_{i1k1} \frac{\partial \hat{v}^k}{\partial \hat{x}_1} + \hat{E}\hat{L} \int_{\widehat{\Omega}} \frac{\partial \hat{w}^i}{\partial \hat{x}_s} \hat{C}_{iskt} \frac{\partial \hat{v}^k}{\partial \hat{x}_t}, \quad s \neq 1, t \neq 1, \\
\hat{f}(\hat{v}; \hat{\mu}) &= \int_{\hat{\gamma}_2} \hat{\tau}^2 \hat{v}^2 + \hat{\tau}^3 \hat{v}^3,
\end{aligned}$$

where the superscript i denotes the i-th component of the respective vector and we assume summation on repeated indices. Moreover, $\hat{\gamma}_1 = \{0\} \times (-0.5, 0.5) \times (-0.5, 0.5)$ and $\hat{\gamma}_2 = \{5\} \times (-0.5, 0.5) \times (-0.5, 0.5)$ are the local ports of the component. Note that Young's modulus parameter is "free" as it appears outside the whole integral in the bilinear form. We also define the inner products

$$\begin{aligned}
(\hat{v}, \hat{w})_{\hat{X}} &:= \sum_{i=1}^{3} \int_{\widehat{\Omega}} \frac{d\hat{v}^i}{d\hat{x}_1} \frac{d\hat{w}^i}{d\hat{x}_1} + \frac{d\hat{v}^i}{d\hat{x}_2} \frac{d\hat{w}^i}{d\hat{x}_2} + \frac{d\hat{v}^i}{d\hat{x}_3} \frac{d\hat{w}^i}{d\hat{x}_3}, \\
(\hat{v}, \hat{w}; \hat{\mu})_{\hat{X};\hat{\mu}} &:= \sum_{i=1}^{3} (1/\hat{L}) \int_{\widehat{\Omega}} \frac{d\hat{v}^i}{d\hat{x}_1} \frac{d\hat{w}^i}{d\hat{x}_1} + \hat{L} \int_{\widehat{\Omega}} \frac{d\hat{v}^i}{d\hat{x}_2} \frac{d\hat{w}^i}{d\hat{x}_2} + \frac{d\hat{v}^i}{d\hat{x}_3} \frac{d\hat{w}^i}{d\hat{x}_3},
\end{aligned} \tag{80}$$

and denote with Γ_D the Dirichlet boundary. Finally, we consider the solution space $X = \{v \in H^1(\Omega)^3 : v = 0 \text{ on } \Gamma_D\}$ and obtain well-posedness of the "truth" approximation and hence the Galerkin formulation (35) of the PR-SCRBE method thanks to Korn's inequality.
In order to determine approximations of the constants c^t, c^X, and c_2^X we proceed as in Section 6.1. We choose $\alpha_{app}(\mu)$ as an approximation of the smallest eigenvalue of the Schur complement matrix, where we have set the relative tolerance of the employed Krylov–Schur algorithm to 0.1. For the discretization of `component 1` we employ linear hexahedral finite elements with $\mathcal{N} = 3348$ degrees of freedom (1116 mesh nodes) and a reference port space dimension of $\mathcal{N}_{\mathcal{P}} = 108$. We perform a pairwise training algorithm[4] [18] and subsequently

[4]Following the notation in [18] we have chosen $N_{samples} = 500$ and $\gamma = 1$ in the pairwise training algorithm.

apply a POD to compress the so obtained functions on the ports to 24 port modes. By adding the six modes that span the space of the rigid body modes we obtain 30 empirical port modes both for the Galerkin and the Petrov-Galerkin formulation. We have set the relative tolerance for the Greedy algorithm to 10^{-7}.
Initially, we consider a `system 5` of two components with system parameters $\mu_1 = (1.0, 1.0, 0.4, 0.6)$ and $\mu_2 = (1.0, 1.0, -, -)$, where we remark that the traction is prescribed with respect to reference coordinates. The Petrov-Galerkin PR-SCRBE approximation for $N = N_{max}$ and $n = 108$ is depicted in Fig. 7 and the bending in x_2 and x_3 directions is clearly observable. In Tab. 1 we compare $\alpha_{app}(\mu)$ for the Galerkin and the Petrov-Galerkin formulation of the PR-SCRBE method for $n = 108$ and an increasing number of RB basis functions N with $\alpha^{\mathcal{N}}(\mu)$. We observe that for $N = 2$ the constant $\alpha_{app}(\mu)$ for the Petrov-Galerkin formulation is negative which suggests to increase the number of RB basis functions. In spite of that, we see that for $N \geq 3$ both for the Galerkin and the Petrov-Galerkin formulation the approximations $\alpha_{app}(\mu)$ converge rapidly to a limit of around $2.307751 \cdot 10^{-04}$, which is a very good approximation of the coercivity constant $\alpha^{\mathcal{N}}(\mu)$. For $N = N_{max}$ and $n = 1$ we obtain $\alpha_{app}(\mu) \approx 2.316429 \cdot 10^{-04}$ both for the Galerkin and the Petrov-Galerkin formulation and the approximations merely change for increasing n. We hence conclude that the smallest eigenvalue of the Schur complement matrix may serve in our certification framework both as a reasonable approximation of $\alpha^{\mathcal{N}}(\mu)$ also for small N and n and an additional indicator for the quality of the RB approximation.
Next we compare the convergence behavior of $\|u(\mu) - u_n^N(\mu)\|_X^{rel}$ and $\Delta_{rel}^1(\mu)$ for $N = N_{max}$ and an increasing number of port modes n for the Galerkin and the Petrov-Galerkin formulation (cf. Fig. 8a). For both cases we observe a rather rapid convergence of the empirical port modes, for instance for $n = 20$ we already obtain a relative error of less than 10^{-4}. Due to the very small coercivity constant we obtain a rather large effectivity constant $\eta^1(\mu)$, which has of course to be taken into account when employing $\Delta^1(\mu)$ as a stopping criterion. However, we see that for both formulations the error estimator $\Delta^1(\mu)$ provides an effective bound as it features the same convergence rate as the relative error. If we consider $n = 108$ port modes and increase the number of RB basis functions, we see that for the Galerkin formulation the estimator increases if we enhance $N = 1$ to $N = 2$ and that the relative error only drops slightly (cf. Fig. 8b). Apart from that $\Delta^1(\mu)$ describes the behavior of the error very well. For the Petrov-Galerkin formulation we detect a slight increase of the effectivity $\eta^1(\mu)$ for increasing N (cf. Fig. 8b). Considering $n = 20$ port modes and an increasing N, we observe in Fig. 8c that for the Galerkin formulation and $N \geq 3$ the effectivity is nearly constant. Considering the same choices of n and N for the Petrov-Galerkin formulation in Fig. 8d, we see that $\|u(\mu) - u_n^N(\mu)\|_X^{rel}$ stagnates for $N = 7$ and $\Delta_{rel}^1(\mu)$ for $N = 6$ which causes a slight increase in the effectivity $\eta^1(\mu)$. Apart from that we see that $\Delta^1(\mu)$ captures the behavior of the dominant model error well. Note that the stagnation of both the error and $\Delta^1(\mu)$ in Fig. 8c and Fig. 8d is due to the usage of only $n = 20$ port modes resulting in a domination of the port reduction error. We therefore conclude that also for this test case the error estimator $\Delta^1(\mu)$ provides an effective bound which may be employed to balance the error contributions between the PR and RB errors. The inferior sharpness compared to the previous test case is due to the small coercivity constant. Note that this matches the theoretical results from the previous section and is thus in some sense an anticipated behavior.
Comparing the approximation properties of the Galerkin and the Petrov-Galerkin formulation for $n = 108$ (cf. Fig. 8b) and $n = 20$ (cf. Fig. 8d), we observe that as expected the Galerkin formulation yields a faster convergence for increasing N. However by using at most 3 additional RB basis functions we obtain for the Petrov-Galerkin, which is more favorable from a computational viewpoint (see §5), the same accuracy as for the Galerkin formulation. We hence infer that both formulations provide at least for the considered test case a rapid convergent approximation.
To analyze the constants in $\Delta^1(\mu)$ and $\eta^1(\mu)$ due to a geometric transformation we consider a `system 6` of two components with parameter configurations $\mu_1 = (1.0, L, 0.2, 0.3)$ and $\mu_2 = (1.0, L, -, -)$ and varying length scaling parameter L. We use the Petrov-Galerkin formulation. Note that in contrast to the previous

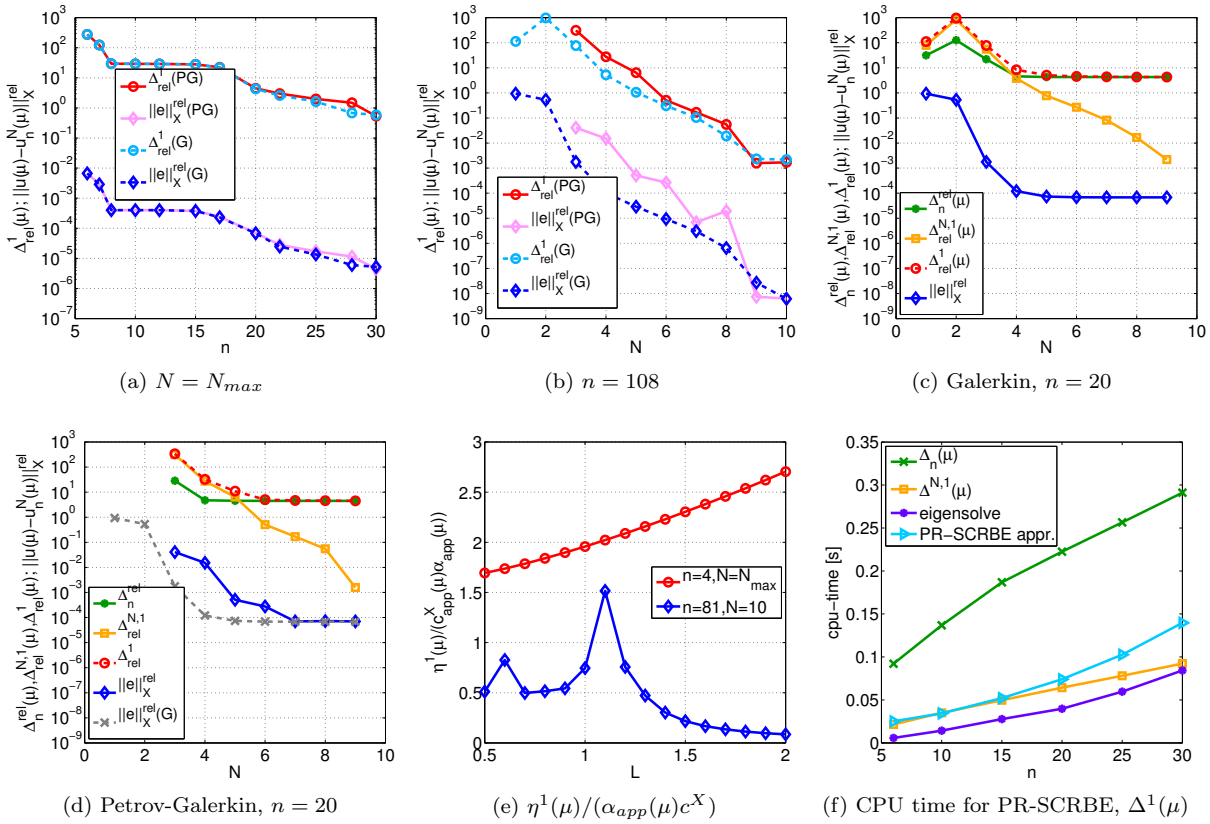

(a) $N = N_{max}$ (b) $n = 108$ (c) Galerkin, $n = 20$

(d) Petrov-Galerkin, $n = 20$ (e) $\eta^1(\mu)/(\alpha_{app}(\mu)c^X)$ (f) CPU time for PR-SCRBE, $\Delta^1(\mu)$

Figure 8: `system 5`: Comparison of the behavior of $\Delta^1_{rel}(\mu)$ and $\|u(\mu) - u_n^N(\mu)\|^{rel}_X$ for the Galerkin (G) and the Petrov-Galerkin (PG) formulation of the PR-SCRBE method (a)-(d); $e := u(\mu) - u_n^N(\mu)$; `system 6`: $\eta^1(\mu)/(\alpha_{app}(\mu)c^X)$ for a varying length scaling parameter L (e); CPU time for the PR-SCRBE approximation and $\Delta^1(\mu)$ for `system 7` and increasing n and $N = 10$ (f)

test case the length scaling stronger affects the behavior of the solution. We see in Fig. 8e that for $n = 20$ and $N = N_{max}$ the effectivity $\eta^1(\mu)/(\alpha_{app}(\mu)c^X)$ slightly increases for growing L. Employing c^t instead of c^t_{app} mitigates this effect but we still observe an slight increase. Considering $n = 108$ and $N = 7$ we detect a stronger variation of $\eta^1(\mu)$ for growing L. However as the ratio between the highest value of $\eta^1(\mu)$ for $L = 1.1$ and its smallest value for $L = 2.0$ is smaller than 20 the deviations are still within a reasonable range.

At last we investigate the online computational costs and consider for that purpose a `system 7` with 5 components and component parameters $\mu_1 = (2.0, 1.0, 0.3, 0.2)$ and $\mu_2 = \mu_3 = \mu_4 = \mu_5 = (2.0, 1.0, -, -)$. As in our current implementation Dirichlet boundary conditions affect the component configuration we have $I_{eff} = 3$. Comparing the online CPU time of the Petrov-Galerkin PR-SCRBE approximation and $\Delta^1(\mu)$ for $N = 10$ and increasing n we see that the PR-SCRBE approximation scales on average quadratically in n (cf. Fig.8f). Both for $\Delta_n(\mu)$ and $\Delta^{N,1}(\mu)$ we detect a linear scaling, which is compliant with the operation counts discussed in §5. Thanks to the additional costs for the eigensolve the portion of the online costs of the error estimator $\Delta^{N,1}(\mu)$ amounts to approximately 82%. Thus we infer that the estimator is also for this test case computable at reasonable additional online costs.

The computation of the corresponding "truth" FE approximation required on average 14.75 seconds, where we have used a conjugate gradient method with relative tolerance 10^{-08}. For the solution of the Schur complement system we have employed a stabilized bi-conjugate gradient method with the same relative tolerance. The computation of a certified PR-SCRBE approximation with a relative error of $8.30531 \cdot 10^{-06}$ took on average 0.4 seconds. Also for this system we obtain a high effectivity $\eta^1(\mu)$ due to $\alpha_{app}(\mu) \approx 1.863954 \cdot 10^{-05} \leq \alpha^{\mathcal{N}}(\mu) \approx 1.104764 \cdot 10^{-04}$ which remains however constant for increasing n. Again the tendency of the error estimator $\Delta^1(\mu)$ to overestimate the error due to the small coercivity constant affects the applicability of $\Delta^1(\mu)$ as a stopping criterion and hence limits to some extent the computational savings that may be realized in the online stage.

7. Conclusions

In this paper we have introduced a new certification framework for the port reduced static condensation method (PR-SCRBE) which provides a rigorous and effective bound. By adapting the concept of conservative fluxes introduced in [19] to the PR-SCRBE setting we have derived an a posteriori error estimator for port reduction which is based on local indicators associated with the ports. To combine this estimator with the estimator for the RB error, which is based on component-local indicators that are the norms of weighted Riesz representations, we have exploited the orthogonality of the component interior "bubble" function space and the coupling modes on the archetype components. We have derived upper bounds for the effectivities both for the local PR and RB indicators and the PR and RB error estimators.
The numerical experiments for heat conduction and isotropic linear elasticity demonstrate that the introduced estimator is indeed an effective bound both for the error caused by the Galerkin and the Petrov-Galerkin formulation of the PR-SCRBE method and also for systems containing components subject to non-orthogonal geometric transformations. However, while the error estimator provides a sharp bound for heat conduction problems the effectivities for the considered problem in linear elasticity are rather high due to the unfavorable coercivity constant. The experiments also show that the local indicators are effective and that the effectivities change only slightly for varying non-geometric parameters. Moreover for the considered test cases the local indicators have predicted the error distribution on the components (RB indicator) and ports (PR indicator) reasonably well. This demonstrates their potential for being employed within an adaptive PR-SCRBE scheme, which is subject of future work. Finally, the error estimator captures the interaction between the PR and RB errors very well and thus allows us to balance both error contributions in the online stage.
We hence conclude that the introduced a posteriori error estimator facilitates both an efficient error control for moderate coercivity constants and an efficient and (locally) adaptive choice of the dimension of the RB and PR spaces. As the numerical experiments show that the error estimator is computable at reasonable additional online costs, the estimator thus enables us to realize significant online computational savings.

Acknowledgements

I would like to thank Prof. Anthony Patera for many insightful discussions and comments on the content of this paper. I am grateful to Dr. David Knezevic for the development of the SCRBE library code and to Dr. Jens Eftang for fruitful discussions. This work was supported by OSD/AFOSR/MURI Grant FA9550-09-1-0613 and ONR Grant N00014-11-1-0713 and the Chaire d'Excellence of the Fondation Sciences Mathématiques de Paris.

Appendix A. $H^{1/2}$-orthonormal port modes

We may alternatively consider port modes which are orthonormal with respect to a $H^{1/2}$-inner product. As the computation of the inner product corresponding to the Sobolev–Slobodeckij-norm (cf. [40]) is com-

putationally challenging we introduce instead an implicitly defined $H^{1/2}$-inner product, which is defined via an extension operator to the archetype (reference) component. In detail we introduce for each local port $\hat{\gamma}_j$, $j = 1, ..., P^\gamma$, an extension operator $\hat{\mathfrak{R}}_j : \hat{\Lambda}_j^{\mathcal{N}_p} \to \hat{X}^{\mathcal{N}}$, with $\hat{\mathfrak{R}}_j v = 0$ on $\hat{\gamma}_{j'}$ for $j \neq j'$, and then define an $H^{1/2}$-inner product as

$$(\hat{\zeta}, \hat{\kappa})_{H^{1/2}(\hat{\gamma}_j)^{d_r}} := (\hat{\mathfrak{R}}_j \hat{\zeta}, \hat{\mathfrak{R}}_j \hat{\kappa})_{\hat{X}} \quad \forall \hat{\zeta}, \hat{\kappa} \in \hat{\Lambda}_j^{\mathcal{N}_p}. \tag{A.1}$$

The application of the trace theorem yields that $(\cdot, \cdot)_{H^{1/2}(\hat{\gamma}_j)^{d_r}}$ is positive definite and hence indeed an inner product on the space $\hat{\Lambda}_j^{\mathcal{N}_p}$. Note that for the trace operator $\mathfrak{T}_j : X^{\mathcal{N}} \to \hat{\Lambda}_j^{\mathcal{N}_p}$ the set $\{\mathfrak{T}_j \hat{\mathfrak{R}}_j \hat{\chi}_{j,k}\}_{k=1}^{\mathcal{N}_\mathcal{P}}$ is a Riesz basis for $\hat{\Lambda}_j^{\mathcal{N}_p}$.

To compute the respective port modes within the pairwise training algorithm we extract functions on the port for each parameter value of the train sample[5] and subsequently compute the lifting to the reference component. Note that this step requires $\mathcal{O}(N_{samples}[P^\gamma \mathcal{N}_\mathcal{P}(QN^2 + N^3) + (P^\gamma \mathcal{N}_\mathcal{P})^2 QN + \mathcal{N}^\sigma])$ operations for the Petrov-Galerkin and $\mathcal{O}(N_{samples}[P^\gamma \mathcal{N}_\mathcal{P}(QN^2 + N^3) + (P^\gamma \mathcal{N}_\mathcal{P})^2 QN^2 + \mathcal{N}^\sigma])$ operations for the Galerkin formulation as we employ a non port reduced SCRBE approximation to compute the functions on the ports. Here $N_{samples}$ denotes the size of the train sample and σ depends on the employed solver to compute the extension. We remark that in general we expect the computational costs for the lifting to be rather small as for most snapshots on the port the extension will have support only within a small part of the component. To guarantee that we obtain the full port space we also add extensions of Legendre modes. The latter can be obtained by solving a singular eigenvalue problem in the complement space of the empirical modes [15, 18]. Finally, we apply a POD to the extensions to determine the principal components. Note that the formation of the Gramian can be performed in $\mathcal{O}(N_{samples}^2 \mathcal{N})$ operations and that the solution of the corresponding eigenvalue problem requires $\mathcal{O}(N_{samples}^3)$ operations.

To define a $H^{1/2}$-inner product for a mapped port $\gamma_{i,j}$ we recall our assumption that $\mathcal{T}_i^{def}$ when applied to a port $\hat{\gamma}_j$ is a pure rigid body motion which we denote for notational convenience with $\mathcal{T}_{i,j}^{rb}$. We also introduce the inner product $(v, v)_{X_{i,j}^{rb}} := ((\mathcal{T}_i^{map})^{-1}(v \circ \mathcal{T}_{i,j}^{rb}), (\mathcal{T}_i^{map})^{-1}(v \circ \mathcal{T}_{i,j}^{rb}); \mu_i)_{\hat{X}}$ and the mapped extensions $\mathfrak{R}_{i,j}\kappa \equiv (\mathcal{T}_i^{map})(\hat{\mathfrak{R}}_j \hat{\kappa} \circ (\mathcal{T}_{i,j}^{rb})^{-1})$ for all $\hat{\kappa} \in \hat{\Lambda}_j^{\mathcal{N}_p}$. Then we obtain

$$(\hat{\mathfrak{R}}_j \hat{\xi}, \hat{\mathfrak{R}}_j \hat{\kappa})_{\hat{X}_j} = (\mathfrak{R}_{i,j}\xi, \mathfrak{R}_{i,j}\kappa)_{X_{i,j}^{rb}}$$

and may thus define

$$(\zeta, \kappa)_{H^{1/2}(\gamma_{i,j})^{d_r}} := (\hat{\zeta}, \hat{\kappa})_{H^{1/2}(\hat{\gamma}_j)^{d_r}} = (\hat{\mathfrak{R}}_j \hat{\zeta}, \hat{\mathfrak{R}}_j \hat{\kappa})_{\hat{X}} \quad \forall \zeta, \kappa \in \Lambda_{i,j}^{\mathcal{N}_p}. \tag{A.2}$$

Note that thanks to this definition we obtain port modes that are $H^{1/2}$-orthonormal on each global port Γ_p, $p = 1, ..., P^\Gamma$ within the system in physical coordinates. The conservative flux may be defined as in (47), with the L^2-inner product replaced by the $H^{1/2}$-inner product (A.2). Thanks to the definition (A.2) and the so maintained orthonormality of the port modes the computation of the conservative flux again reduces to the calculation of the euclidean norm of the vector associated with the residual in (48). If we allow geometric mappings that deform the port the computational costs increase as discussed in Section 5. The estimate for part II in the proof of Proposition 4.2 can be done in an analogous manner. Note that the constant c^t has to be modified. The effectivity $\eta_n(\mu)$ can now be bounded as follows.

[5] Note that the parameter here additionally accounts for the parametrization of the boundary conditions on the non-shared port. For further details we refer to [15, 18].

Corollary Appendix A.1. *For $H^{1/2}$-orthonormal port modes the local error indicators $\Delta_n^p(\mu)$ may be bounded as*

$$\Delta_n^p(\mu) \leq \nu^{\mathcal{N}}(\mu)\tilde{C}_p \|u(\mu) - u_n^N(\mu)\|_{X_i \oplus X_{i'}}, \quad \text{for } \pi_p = \{(i,j),(i',j')\}. \tag{A.3}$$

Furthermore the effectivity $\eta_n(\mu)$ satisfies

$$\eta_n(\mu) \leq \frac{\nu^{\mathcal{N}}(\mu)}{\alpha_{app}(\mu)} c_{app}^t c_{app}^X \sqrt{P^\gamma} \max_{p=1,\ldots,P^\Gamma} \tilde{C}_p. \tag{A.4}$$

Proof. The proof follows the lines of the proof of Proposition 4.5 but does not require the application of the inverse estimate. □

References

[1] W. C. Hurty, Dynamic analysis of structural systems using component modes, AIAA journal 3 (4) (1965) 678–685.

[2] M. Bampton, R. Craig, Coupling of substructures for dynamic analyses., AIAA Journal 6 (7) (1968) 1313–1319.

[3] F. Bourquin, Component mode synthesis and eigenvalues of second order operators: discretization and algorithm, RAIRO Modél. Math. Anal. Numér. 26 (3) (1992) 385–423.

[4] U. Hetmaniuk, R. B. Lehoucq, A special finite element method based on component mode synthesis, ESAIM Math. Model. Numer. Anal. 44 (3) (2010) 401–420.

[5] H. Jakobsson, F. Bengzon, M. G. Larson, Adaptive component mode synthesis in linear elasticity, Internat. J. Numer. Methods Engrg. 86 (7) (2011) 829–844.

[6] Y. Maday, E. M. Rønquist, The reduced basis element method: application to a thermal fin problem, SIAM J. Sci. Comput. 26 (1) (2004) 240–258 (electronic).

[7] G. Rozza, D. B. P. Huynh, A. T. Patera, Reduced basis approximation and a posteriori error estimation for affinely parametrized elliptic coercive partial differential equations: application to transport and continuum mechanics, Arch. Comput. Methods Eng. 15 (3) (2008) 229–275.

[8] R. DeVore, G. Petrova, P. Wojtaszczyk, Greedy algorithms for reduced bases in Banach spaces, Constr. Approx. 37 (3) (2013) 455–466.

[9] L. Iapichino, A. Quarteroni, G. Rozza, A reduced basis hybrid method for the coupling of parametrized domains represented by fluidic networks, Comput. Methods Appl. Mech. Engrg. 221/222 (2012) 63–82.

[10] I. Maier, B. Haasdonk, A Dirichlet–Neumann reduced basis method for homogeneous domain decomposition problems, Appl. Numer. Math. 78 (2014) 31–48.

[11] N. C. Nguyen, A multiscale reduced-basis method for parametrized elliptic partial differential equations with multiple scales, J. Comput. Phys. 227 (23) (2008) 9807–9822.

[12] F. Schindler, B. Haasdonk, S. Kaulmann, M. Ohlberger, The localized reduced basis multiscale method, in: Proceedings of Algoritmy 2012, Conference on Scientific Computing, Vysoke Tatry, Podbanske, September 9-14, 2012, Slovak University of Technology in Bratislava, Publishing House of STU, 2012, pp. 393–403.

[13] Y. Efendiev, J. Galvis, T. Y. Hou, Generalized multiscale finite element methods (GMsFEM), Journal of Computational Physics 251 (2013) 116–135.

[14] D. B. P. Huynh, D. J. Knezevic, A. T. Patera, A static condensation reduced basis element method: approximation and *a posteriori* error estimation, ESAIM Math. Model. Numer. Anal. 47 (1) (2013) 213–251.

[15] J. L. Eftang, A. T. Patera, Port reduction in parametrized component static condensation: approximation and a posteriori error estimation, Internat. J. Numer. Methods Engrg. 96 (5) (2014) 269–302.

[16] S. Vallaghé, A. T. Patera, The static condensation reduced basis element method for a mixed-mean conjugate heat exchanger model, SIAM J. Sci. Comput. 36 (3) (2014) B294–B320.

[17] D. B. P. Huynh, D. J. Knezevic, A. T. Patera, A static condensation reduced basis element method: Complex problems, Comput. Methods Appl. Mech. Engrg. 259 (2013) 197–216.

[18] J. L. Eftang, A. T. Patera, A port-reduced static condensation reduced basis element method for large component-synthesized structures: approximation and *A posteriori* error estimation, Advanced Modeling and Simulation in Engineering Sciences 1 (3) (2013).

[19] T. J. R. Hughes, G. Engel, L. Mazzei, M. G. Larson, The continuous Galerkin method is locally conservative, J. Comput. Phys. 163 (2) (2000) 467–488.

[20] M. G. Larson, A. Målqvist, Adaptive variational multiscale methods based on a posteriori error estimation: energy norm estimates for elliptic problems, Comput. Methods Appl. Mech. Engrg. 196 (21-24) (2007) 2313–2324.

[21] P. Henning, M. Ohlberger, B. Schweizer, An Adaptive Multiscale Finite Element Method, Multiscale Model. Simul. 12 (3) (2014) 1078–1107.

[22] A. Målqvist, D. Peterseim, Localization of elliptic multiscale problems, Math. Comp. 83 (290) (2014) 2583–2603.

[23] M. Ohlberger, F. Schindler, A-posteriori error estimates for the localized reduced basis multi-scale method, in: Finite Volumes for Complex Applications VII—Methods and Theoretical Aspects, Springer International Publishing, 2014, pp. 421–429.

[24] M. Barrault, Y. Maday, N. Nguyen, A. Patera, An 'empirical interpolation' method: application to efficient reduced-basis discretization of partial differential equations, C. R. Math. Acad. Sci. Paris Series I 339 (2004) 667–672.

[25] A. Quarteroni, A. Valli, Domain decomposition methods for partial differential equations, Numerical Mathematics and Scientific Computation, The Clarendon Press Oxford University Press, New York, 1999, oxford Science Publications.

[26] K. Veroy, C. Prud'homme, D. V. Rovas, A. T. Patera, A posteriori error bounds for reduced-basis approximation of parametrized noncoercive and nonlinear elliptic partial differential equations, in: Proceedings of the 16th AIAA Computational Fluid Dynamics Conference, Vol. 3847, 2003.

[27] A. Ern, J. Guermond, Theory and practice of finite elements, Vol. 159 of Applied Mathematical Sciences, Springer-Verlag, New York, 2004.

[28] I. Babuška, A. Miller, The post-processing approach in the finite element method—part 1: Calculation of displacements, stresses and other higher derivatives of the displacements, Int. J. Numer. Methods Eng. 20 (6) (1984) 1085–1109.

[29] P. M. Gresho, R. L. Lee, R. L. Sani, M. K. Maslanik, B. E. Eaton, The consistent galerkin fem for computing derived boundary quantities in thermal and or fluids problems, Internat. J. Numer. Methods Fluids 7 (4) (1987) 371–394.

[30] A. Toselli, O. Widlund, Domain decomposition methods—algorithms and theory, Vol. 34 of Springer Series in Computational Mathematics, Springer-Verlag, Berlin, 2005.

[31] T. P. A. Mathew, Domain decomposition methods for the numerical solution of partial differential equations, Vol. 61 of Lecture Notes in Computational Science and Engineering, Springer, 2008.

[32] S. Vallaghé, D. B. P. Huynh, D. J. Knezevic, A. T. Patera, Component-based reduced basis for eigenproblems, Tech. Rep. 61, MechE, MIT (USA) (2013).
URL `http://augustine.mit.edu/methodology/papers/VHKP_CS_July2013.pdf`

[33] G. Strang, G. Fix, An analysis of the finite element method, 2nd Edition, Wellesley-Cambridge Press, Wellesley, MA, 2008.

[34] S. I. Repin, Computable majorants of constants in the Poincaré and Friedrichs inequalities, Journal of Mathematical Sciences 186 (2) (2012) 1–15.

[35] L. E. Payne, H. F. Weinberger, An optimal Poincaré inequality for convex domains, Archive for Rational Mechanics and Analysis 5 (1) (1960) 286–292.

[36] J.-L. Lions, E. Magenes, Non-homogeneous Boundary Value Problems and Applications 1, Springer-Verlag Berlin, 1972.

[37] B. S. Kirk, J. W. Peterson, R. H. Stogner, G. F. Carey, libMesh: A C++ library for parallel adaptive mesh refinement/coarsening simulations, Engineering with Computers 22 (3-4) (2006) 237–254.

[38] D. J. Knezevic, J. W. Peterson, A high-performance parallel implementation of the certified reduced basis method., Comput. Methods Appl. Mech. Eng. 200 (13-16) (2011) 1455–1466.

[39] V. Hernandez, J. E. Roman, V. Vidal, SLEPc: a scalable and flexible toolkit for the solution of eigenvalue problems, ACM Trans. Math. Software 31 (3) (2005) 351–362.

[40] R. A. Adams, Sobolev spaces, Academic Press, New York-London, 1975, pure and Applied Mathematics, Vol. 65.